POLITECNICO DI MILANO

Scuola di Ingegneria Industriale e dell'Informazione

Corso di studi in

Engineering Physics – Nanophysics and Nanotechnology

The role of Reactive Oxygen Species in smart bio - organic interfaces

Relatore: Prof. Guglielmo Lanzani

Correlatore: Dr. Maria Rosa Antognazza

Elaborato finale di

Ilaria Abdel Aziz

Matricola 837195

AA 2015/2016

Index of contents

List of figures

List of tables

Abstract (English)

Polymer nanoparticles have a huge potential application in biotechnology and medicine. Recently, it has been demonstrated that organic semiconductors can reliably control the electrical activity of living cells and tissues. In particular, polythiophene NPs have been reported to enhance light sensitivity in Hydra Vulgaris animal model, with sizable effects on their behaviour and gene expression. However, the mechanisms behind polymer-based photo-transduction remain unclear. In this work, we extensively considered, as a possible transduction mechanism, the enhancement of physiological levels of Reactive Oxygen Species, at non-toxic levels. We provide evidences of ROS production in both cell and Hydra models, and we relate it to altered calcium signalling dynamics. Based on the present results, a model for photo – activation mechanism is presented and critically discussed.

Abstract (Italian)

La sintesi di nanoparticelle di polimero ha aperto interessanti possibilità nei campi della biotecnologia e della medicina. Recentemente è stato dimostrato che tramite semiconduttori organici, è possibile controllare e modulare l'attività di tessuti e cellule viventi. In particolare, sono state recentemente utilizzate nanoparticelle di politiofene in un modello di animale invertebrato (*Hydra Vulgaris*), ottenendo importanti effetti sia comportamentali sia di modulazione dell'espressione di specifici geni (opsine). Tuttavia, il meccanismo responsabile del processo di fototrasduzione è tutt'ora oscuro, in modelli *in vitro* così come *in vivo*. In questo lavoro, l'aumento dei livelli fisiologici di specie reattive con l'ossigeno (ROS) viene indagato come possibile spiegazione. Sono stati presi in considerazione un modello cellulare (Human Embryonic Kidney cells, HEK-293) ed un modello animale di invertebrato (*Hydra Vulgaris*). I risultati sperimentali mostrano una più intensa produzione di ROS nel caso di campioni trattati con nanoparticelle e soggetti ad illuminazione, sebbene a livelli non tossici, accompagnata da un'alterata dinamica di calcio intracellulare. Sulla base dei risultati ottenuti, viene presentato e criticamente discusso un possibile modello del processo di fototrasduzione.

Estratto descrittivo in lingua italiana

La realizzazione di interfacce ibride funzionali tra materiali organici e sistemi biologici (colture cellulari, tessuti, e anche animali vertebrati) ha recentemente attratto notevole attenzione per le molteplici, possibili applicazioni in ambito biotecnologico e clinico. Alcuni esempi includono la realizzazione di biosensori di elevata specificità e sensibilità, transistor a effetto campo per la misura e la stimolazione di potenziali d'azione, dispositivi elettrochimici per il rilascio di specifici farmaci e neurotrasmettitori, transistor per e stimolazione in vivo dell'attività cerebrale. In particolare, i polimeri basati su monomeri di tiofene sono stati largamente considerati per le loro eccellenti proprietà optoelettroniche, la versatilità e soprattutto l'elevato grado di biocompatibilità, largamente dimostrata in numerosi studi. In particolare, dispositivi planari costituiti da film sottili di poli-hexyl-tiofene (P3HT) sono stati proposti per modulare (eccitare o inibire) otticamente, nello spettro della luce visibile, l'attività elettrica di cellule e tessuti *in vitro*. Il medesimo approccio ha portato recentemente alla realizzazione di protesi retiniche, in grado di ristabilire l'acuità visiva in ratti geneticamente ciechi. Sfortunatamente, il corretto posizionamento nello spazio sotto-retinico, al posto dei fotorecettori danneggiati, di tali protesi richiede un complesso intervento chirurgico, delicato e potenzialmente molto invasivo. La realizzazione di nanoparticelle funzionali polimeriche, iniettabili nella zona di interesse, permetterebbe di ovviare in modo semplice a questa importante limitazione. In un promettente studio preliminare, è stato osservato che nanoparticelle di P3HT inducono sensibilità alla luce in un modello animale di invertebrato (*Hydra Vulgaris*), con importanti effetti sia comportamentali sia di espressione di specifici geni (opsine). Tuttavia, il processo di fototrasduzione attivo all'interfaccia tra polimero e componente biologica è ancora largamente incompreso, soprattutto nel caso dei sistemi *in vivo* fino ad ora considerati.

In questo scenario, questo lavoro di tesi ha avuto l'obiettivo di caratterizzare e comprendere il meccanismo di fototrasduzione attivo all'interfaccia tra le nanoparticelle e il sistema biologico. In particolare, l'attenzione è stata focalizzata sulla possibile attivazione di specifiche reazioni foto-elettrochimiche.

Studi preliminari su film sottili polimerici a contatto con elettroliti salini hanno infatti dimostrato che il materiale attivo, in presenza di luce, reagisce con l'ossigeno

molecolare disciolto in acqua, generando una fotocorrente. Lo scopo di questo lavoro è stato quindi (i) di chiarire se simili reazioni avvengano anche nel caso di nanoparticelle in dispersione acquosa, (ii) se tali processi fotoelettrochimici possano generare la produzione, diretta o indiretta, di specie reattive con l'ossigeno (ROS)in ambiente intracellulare, così come in modelli animali semplici di Hydra Vulgaris, e (iii) se le specie elettrochimiche eventualmente prodotte interferiscano in qualche modo con l'attività fisiologica della cellula.

Gli esperimenti condotti hanno permesso di realizzare gli obiettivi preposti. In particolare, studi di elettrochimica con elettrodi appositamente funzionalizzati hanno permesso di identificare la fotoproduzione del radicale superossido da parte di nanoparticelle di P3HT illuminate con luce visibile. La misura diretta delle ROS prodotte in ambiente intracellulare è stata effettuata mediante l'uso combinato di probes specifici, sensibili a diverse specie ossidative. Uno studio simile è stato condotto anche in vivo, evidenziando anche in quel caso la produzione di ROS. Infine, si è preso in considerazione l'effetto biologico della sovrapproduzione di ROS, evidenziando in particolare la mutua interazione tra fenomeni fotoelettrochimici e le dinamiche di ioni calcio intracellulare.

La caratterizzazione delle nanoparticelle di politiofene apre un ampio spettro di possibili applicazioni, essendo uno strumento di fotoattuazione. La possibilità di iniettarle rende la loro somministrazione esente da invasività, al contrario di device basati su film di polimero. Inoltre, sono del tutto indipendenti da forme di alimentazione esterna. Gli effetti sull'omeostasi di ioni calcio apre la prospettiva di allargare a cellule eccitabili lo studio, presentando queste una maggiore versatilità nella modulazione di canali atti a regolare le funzioni cellulari.

In memory of my beloved grandmother, always walking next to me, even without being here.

I. Introduction

There are many ways to influence cellular behaviour by external stimuli: electromagnetic, thermal and mechanical ones have been widely studied for years, leading to technological tools for medical applications, like diagnostic or recovery ones. Optical methods have been recently discovered to be optimal tools for diagnosis, for their non – invasiveness and high spatio – temporal resolution. The application of light as stimulus for cellular response has not been largely investigated, mainly because animal cells do not exhibit light sensitivity on their own. Therefore, the development of tools for sensitization is mandatory. A research on this field is being carried, exploiting the properties of organic semiconductors as active layers for the optical actuators, based on photovoltaic processes. The latter concerns the generation of a current (and a voltage) as a consequence of the photon mediated generation of an electron – hole pair inside an active layer. Therefore, the device is made of a film of active layer sandwiched between two electrodes, maintaining the circuit opened. Is straightforward to understand the potential biological applications, being this system free from power sources. Organic semiconductors are eligible materials for their biocompatibility, ease of synthetization and handle. Moreover, they can transport both ions and electrons, that is mandatory since cells communicate exchanging ionic currents. Promising results report on augmented cell responsivity and recovery of vision acuity by blind rats both mediated by poly – 3 – hexyl – thiophene (P3HT) – based devices, even though no explanation about its mechanisms has been provided.

This work aims at explaining this mechanism considering the intervention of polymer generated charges with physiological levels of Reactive Oxygen Species. They influence calcium levels, therefore a possible interaction model is provided. It is divided in three sections: the first chapter gives a background for the problem, describing the interaction between light and tissues and giving some bases about conjugated polymers and their photoexcitation. Then, two different interfaces are characterized: polymer/water and polymer/cell/water one, being related to our experimental setup. Follows a general description of Reactive Oxygen Species and Ca^{2+} roles in cell's activities, concluding the introduction. The second chapter is dedicated to instrumentation and materials used for carrying out the experiments; a short section is dedicated to cells and *Hydra Vulgaris* handle. The third chapter is dedicated to experimental results and discussion, providing different models that explain the achieved outcomes.

I.I Signal Photo – transduction

Interaction with light offers a wide variety of phenomena, mainly depending on frequency, intensity and exposure. The effects of light passing through a dispersive medium are mainly related to scattering and absorption. These processes are useful for image reconstruction, since escaping photons carry information as scattering angle and intensity. This is the basis of optical diagnostic techniques, such as X-ray imaging. When dealing with visible light, is mandatory to consider that many components of human tissues are absorber: haemoglobin and related compounds, melanin and so on are natural chromophores, as reported in figure I.1. Different researches are being

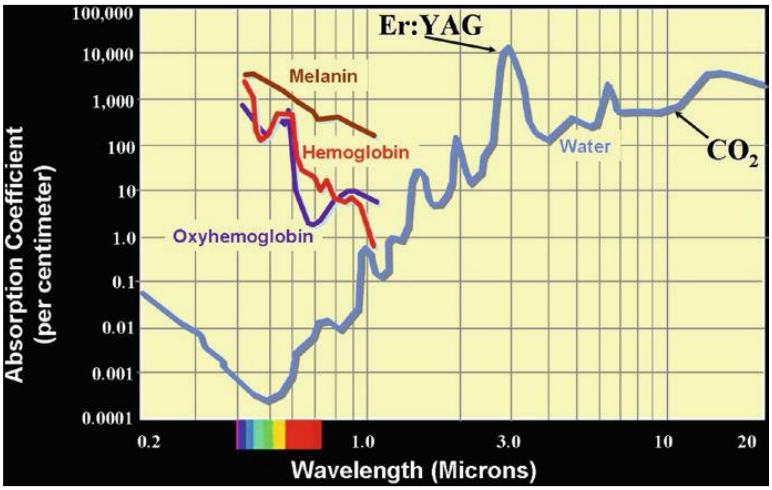

Figure I.1 Absorption coefficient of the main components of human tissues. The figure presents the absorption coefficient vs wavelength of the components of the tissues, as haemoglobin, melanin, oxyhaemoglobin and water. The first three are strong absorber in the visible range of light.

carried in this view: for example, the estimation of tissue components as oxy – deoxy – haemoglobin, lipids and water is a reliable imaging technique for breast imaging [1]. Besides imaging, light can induce effects on cell life and signalling when coupled with chemicals [2]. This is the case of the photodynamic therapy: this promising approach is very attractive for treating cancer, because of its specificity and selectivity. Basically, a chemical compound sensitive to light (photosensitizer) is able to specifically bind target proteins: when photoexcited, it reacts with the oxygen present in intracellular environment, increasing the amount of Reactive Oxygen Species (ROS). Physiological concentrations act as a second messenger, responsible for cell signalling. Therefore, photodynamic therapy increases ROS levels up to induce cell death [3]. Photosensitizers can mediate also other kind of mechanisms, since cells' activity can be controlled in many ways: changes in ionic concentration and modifications of thermal gradient [4] can both induce or inhibit cellular functions. Another interesting field of application of

this coupling between optic and chemistry is given by optogenetics: the idea behind it is to achieve a selective control of neurons' activity in intact brains. This is achieved by genetically modifying neurons to express light – sensitive ion channels, obtaining a complete ability of manipulation of neuronal networks' activity [5]. The genetic modification must be carried out with light – sensitive proteins, such as rhodopsin – derived ones. An interesting feature is that rhodopsin is already present in human system, being one of the actors of the vision cascade. Its activation is achieved when 11 – cis – retinal isomerizes to trans form (figure I.2): this process is typical of photochromic compounds. One thing at time: photochromism is a reversible process by which photon absorption is responsible for conformational changes, leading the molecule from cis to trans isomer (or vice versa). When light irradiation ends, the

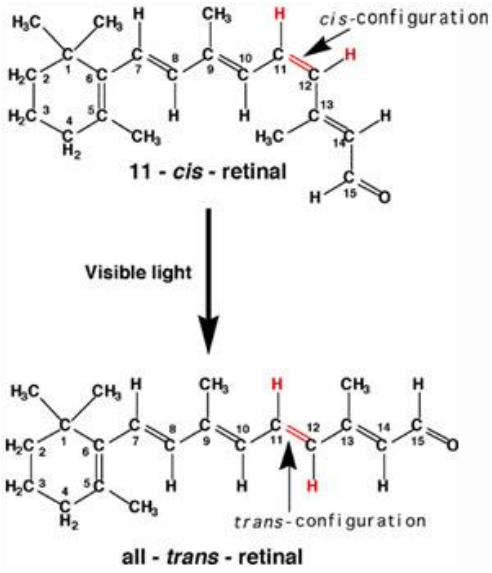

Figure I.2 Cis - Trans isomerization of 11 - cis - retinal. The 11 – cis – retinal undergoes this isomerization when illuminated with visible light. It is a protein found in human eye. As a consequence of the isomerization, it binds other proteins starting the vision cascade (Appendix A).

molecule goes back to its original state. This behaviour is typical of many molecules, nowadays used for applications as sunglasses and memory arrays [6], but is also the trigger for the vision cascade. When no light is impinging on photoreceptors, rhodopsin is accommodated to retinal thanks to its cis geometrical conformation [7]; photon incoming provokes the change in conformation of the retinal, that goes to *all trans* configuration, generating a change in conformation also for opsin. The latter triggers a protein – cascade mechanism that activates the neuronal network (Appendix A). There are many diseases, like macular degeneration, associated with the loss of ability of photoreceptors to detect light, ending in a lack of central vision. Photoreceptors are photo – transducers, since they convert an optical stimulus into a chemical one. Thus,

a good approach for dealing with this problem is to develop a photo – transducer able to trigger similar chemical reactions. In this view, organic semiconductor devices are being developed, for their reactivity to visible light and biocompatibility. Researches shown how conjugated polymer based devices restored vision acuity in blind rats [8], even though the phototransduction mechanism is still unclear.

I.II Conjugated polymers

Inorganic compounds, mainly based on silicon, have been widely used for interfaces with biological tissues: examples are pacemakers or implants used as recording instruments, like electrocardiographs or encephalographs. The rigid crystalline structure of inorganic compounds is a strong limit, since an elastic part can better keep on the movements of the tissues. Moreover, tissues communicate by both exchanging electrons and holes: inorganic compounds present a very good mobility for electron transport, but they almost do not transport holes. These reasons bring the scientific community to exploit new systems for biological interfaces, such as organic compounds: their main feature is the hybridized state of carbon. In this state, electrons can transfer from one π orbital to the other, conferring the property of delocalization. This transfer mechanism is called hopping. It is one of the possible transport mechanisms for conjugated polymers. The higher the number of carbon atom in sp^2 hybridization, the higher the delocalized states for electron transport, the higher the conjugation.

A chain of repeating unit (monomer) is a polymer. Even if the repeating unit can be always the same molecule or many different ones, the central feature is the carbon atom in sp^2 hybridization. Let us now consider the electronic structure: the polymer is formed by covalent bonding between the monomeric units. Thus, σ bonds are related to valence states, while π ones are related to conduction. When the polymer is formed, those orbitals are so close that they can be treated as a continuum: on this basis, we talk about quasi – band structure. Therefore, we can identify a conduction and a valence band and we can distinguish metals, semiconductors and insulators exactly as inorganic compounds. Focusing on semiconductors, in case of inorganic compounds, the top of the valence band and the bottom of the conduction band are simply called E_V and E_c, respectively. For organic compounds, reminding the fact that we are talking about superposition of molecular orbitals and not exactly bands, the top of the valence band is called Highest Occupied Molecular Orbital (HOMO) and the bottom of the conduction band is called Lowest Unoccupied

Molecular Orbital (LUMO). Thus, the energy gap is identified as $E_g = HOMO - LUMO$. Upon excitation, electrons are excited from the valence to the conduction band. Electrons are transported by hopping mechanisms, that provokes a smaller mobility rather than inorganic compounds; conversely, holes are better transported with respect to inorganic materials.

Conjugated compounds can be modelled as two interplaying parts: the skeleton (or backbone) and the side group. The former is made of carbon atoms with their delocalized electrons, while the side group is whatever can be attached to the

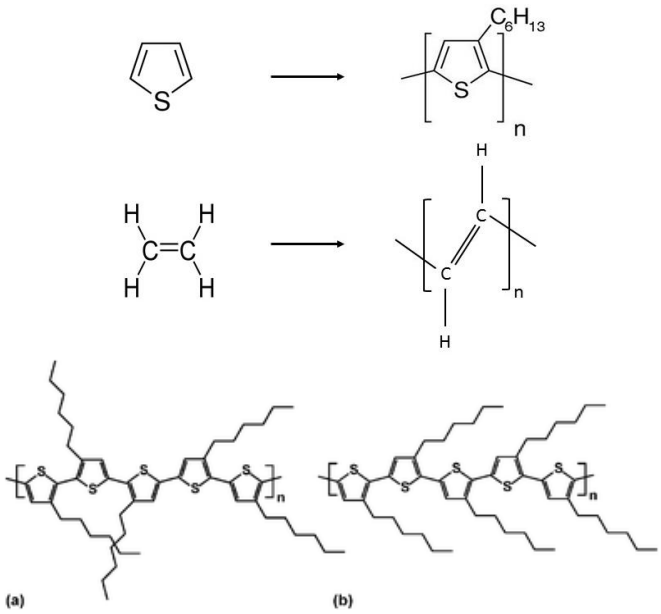

Figure I.3 Monomeric units and related polymers. UP: P3HT polymer has as monomeric unit the thiophene. DOWN: Polyacetylene polymer has as monomeric unit the acetylene. (a) Regiorandom P3HT has the hexyl groups at a random positions of the thipohene ring. (b) Regioregular P3HT has the hexyl groups always in the same position of the thipohene ring.

monomeric unit. The skeleton can have both a linear structure (like ethylene, polymerizing to polyacetylene) or a ring-shaped one (like thiophene, polymerizing to polythiophene), as shown in figure I.3. Focusing on the ring shaped one, depending on the position of the side group, is possible to distinguish between regio-regular and regio-random polymers (figure I.3). The former presents the side group always on the same atom, the latter being the contrary. Regio-regular polymers present a more crystalline like structure, while regio-random one is more amorphous: thus, the former will present a higher mobility with respect to the latter.

One of the most studied polymer is poly-3-hexyl-thiophene (P3HT, since the side group is and hexyl one, as shown in figure I.3) for many reasons: first, it can be easily synthetized, then it has a high absorption cross section and a broad absorption

spectrum in the visible range. Moreover, its biocompatibility has been demonstrated, being even used as photo – transducer in retinal prosthesis implants [8]. A more recently discovered feature of P3HT is the possibility of nanoparticle synthesis [9]: up to now, it has been deposited as thin film, and in the case of retinal prosthesis, it needed surgery for implantation. The form of nanoparticles allows an easy way of administration, avoiding invasiveness. A full characterization of nanoparticles is provided in the following chapters.

Table I.I Excited states of polymers.

	Singlet S_0	Doublet D_1	Triplet T_1
Charge	0	±e	0
Spin	1	$^1/_2$	3
Lifetime	0.01 ÷ 10 ns	10 ps ÷ 10 ms	100 ns ÷10 ms
Wavefunction	Delocalized	Delocalized	Confined (few monomers)
Deactivation	PL S_1 -> S_0 + hv ISC S1 -> T_n IC S_1 -> S_0 + heat	D_1 + D_1 -> S_0 + heat D_1 + D_1 -> S_1 + heat	PH T_1 -> S_0 + hv ISC T_1 -> S_0

The excited states of polymers are a bit different with respect to inorganic compounds' ones, thus a description is required. Is possible to distinguish among three excited states: singlet, doublet and triplet. They are different for charge, spin and relaxation process. Singlet state (S_1) is the lowest excited state above ground (S_0). It is the one from which fluorescence emission occurs, being S_1 - S_0 a dipole-permitted transition. It can be deactivated also by non – radiative paths, such as intersystem crossing (ISC) or internal conversion (IC). Moreover, is the state that collects population relaxing from higher energy states. Doublet state (D_0) is the excited state representing charge carriers. It can be reached by photoexcitation and is deactivated mainly by heat. Triplet state (T_1) can be reached by ISC from higher singlet or triplet excited states. Photoexcitation does not directly reach it since the transition S_0 – T_1 is not permitted by dipole selection rules. It is deactivated by phosphoresce emission or by non – radiative paths. The table below compares some characteristics of those states, as lifetime and charge.

There are also excitations associated with lattice deformations coupling. They can be treated as defects, thus their states are located in the gap of the semiconducting polymer. Mainly, they derive from electron – phonon coupling or electrostatic interaction (in case of polar lattices), being described as wavepackets. The most important are polarons and charge transfer states. Polarons are charge carrier, described as a large quasi-particle delocalized in the lattice. They occur whether bond alternation takes place, thus carrying a spin equal to $^1/_2$ and a charge of ±e. They play a role when the polymer is chemically doped: being a state in the gap, it has a lower energy with respect to valence band electrons, thus the acceptor atom will bind the polaron; for donor atoms is the same, being the polaron state at a lower energy with respect to valence ones. Charge Transfer (CT) states are formed when the interaction between two neighbour molecules generates a static dipole, so these positive and negative regions are bound by Coulomb interaction; they are neutral, spinless quasi – particles. Donor-Acceptor molecules, for example, form CT states upon photoexcitation: they are weakly coupled with the ground state, so they can experience a radiative decay, showing a structure-less emission spectrum. The dissociation of a charge transfer state generates two separate carriers.

Once the excited state is formed, is necessary to talk about photogenerated charges. There are different mechanisms trying to explain how charges dissociate from a charge transfer bound state, all of them being qualitative, since there is not a quantitative theory, yet. It can be modelled as a multi – step process, starting from photon absorption and generation of a neutral excited state; charge carriers are generated by means of autoionization, followed by generation of a bound charge pair due to thermalization, concluding with dissociation into free carriers. The interaction of the charges with the external environment can initiate different processes, as local increase of temperature or electron transfer. All of them are depicted in I.4.

Conjugated polymer nanoparticles (CP-NPs) are raising a high interest in the scientific community for many reasons: first, because they can be obtained by simple synthesis methods, such as ring opening polymerization, radical chain polymerization,

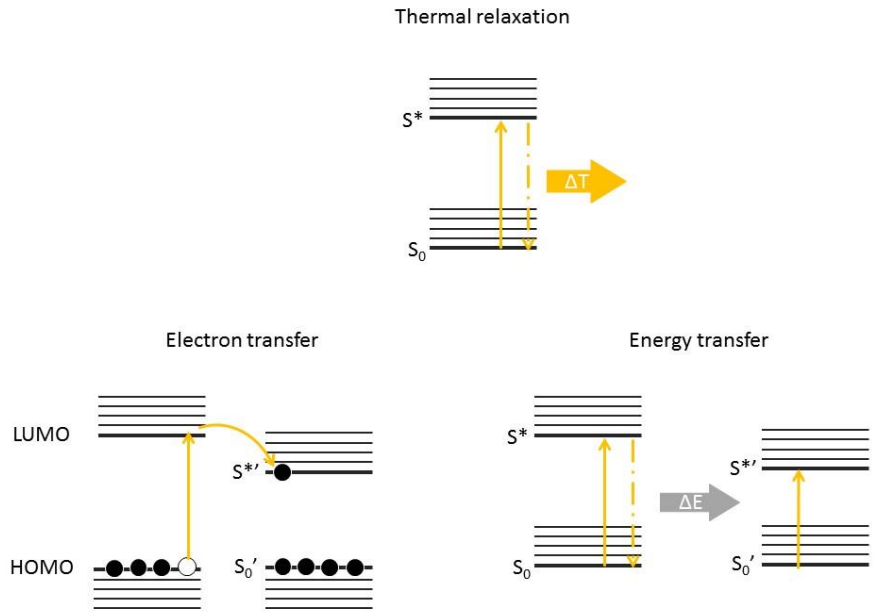

Figure I.4 Mechanisms of polymer - molecules interaction. There are many phenomena that can occur at polymer – molecule interface. **Thermal relaxation** happens when a photoexcited state decays generating heat, that can diffuse around the molecules. **Electron transfer** occurs when the molecule has a lower energy level than the one where lies the photoexcited electron. This provokes the oxidation of the polymer, and so the reduction of the molecule. **Energy transfer** occur when the difference in energy between the polymer levels is closer to the one of an adjacent molecule.

solvent separation and so on. All of them involve a solvent in which the monomeric unit is dissolved. Being synthetized as polymers, their features can be distinguished by looking at side groups and backbone. For which regard the side groups, those CP-NPs present the property of functionalization: during the polymerization, is possible to add functional groups that specifically bind proteins or other compounds, conferring to the final nanoparticle a targeting function. Those functional group can also be fluorescent: once they bind the target protein for example, they start to exhibit fluorescence, giving the possibility of strongly localized diagnostic. Looking at the core, the CP-NPs can be polymerized as a capsule, being able to encapsulate compounds (such as drugs) and to release them locally, for example after having bound a target protein [10]. Presenting also a very low toxicity, they result to be tools for diagnostic and drug delivery. Therefore, being the nanoparticles a good substitute for thin films, their photo-physical properties are a crucial point, especially in aqueous environment. From a physical point of view, CP-NPs electronic excited states are likely molecular ones; thus, they present similar feature with respect to their parent films. Therefore, they possess a good absorption cross section, especially in the visible light range. There is also a strong dependence on morphological and surface structure, both for photo-physical and biological properties. Absorption and emission can be affected by the amount of

crystalline and amorphous phase of the nanoparticle, surface charge and accumulation, while internalization is affected by shape and dimension.

I.III H_2O – polymer interface

Devices made of polymers are being widely used for many application, typically in neuroscience, biomedicine and photo – electrochemical cells. In those cases, the polymer is in contact with aqueous environment, thus a characterization of H_2O – polymer interface is mandatory. Follows a description of polymer interaction with water molecules, based on theoretical molecular models, with oxygen and with hydrogen (water splitting). A detailed description of how an electrochemical experiment is worked out can be found in Appendix B.

As mentioned previously, rr-P3HT (from now on, simply P3HT) is the chosen polymer, thus interaction of both thiophene and hexyl chain with water should be considered. A modelling based on molecular dynamics simulations (MD) and density functional theory (DFT) has been performed [11], focusing on the effect of polarized molecules (water) and on the outcome of oxygen bonding. The former induces a polarization of the polymer outermost surface, provoking a shift towards lower energies of both HOMO and LUMO levels (figure I.5), proportional to the measured

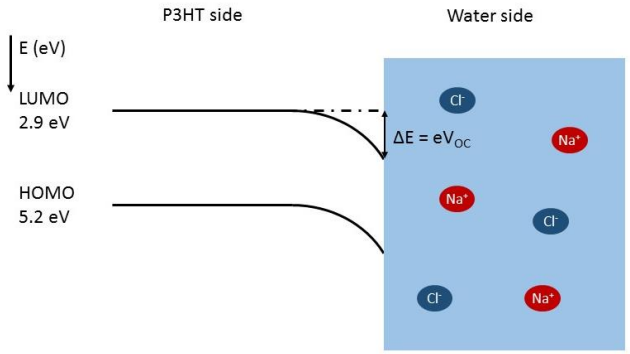

Figure I.5 Band bending of polymer levels at water interface. The interface between polymer and saline environment is characterized by a band bending.

open circuit potential (V_{oc}). It has been reported [11] that the polymer exposes the [010] surface to water, which has some insertion sites for water molecules: therefore, they are able to penetrate for a few angstroms. The interaction with water is weaker than the one of the exposed surface, but can induce as overall effect the interfacial band bending. This polarization orients the LUMO towards the water interface and the HOMO towards the P3HT side. This suggests the exposure of photoexcited electrons towards the water interface. To settle this hypothesis, is possible to perform an

electrochemical measurement of the photocurrent. A thin film of polymer has been spin coated on indium – tin oxide (ITO) – glass slab, contacted to the working electrode of a three-electrodes electrochemical cell (see appendix B for details); the counter electrode (CE) is a Platinum one, while the reference one (RE) is Ag/AgCl. Everything is put in the cell containing an electrolytic solution of NaCl 0.2 M. Measures (figure I.6) show two different effect: in a few subs – seconds, the photovoltage changes its sign from negative to positive, becoming finally positive and reaching a saturation behaviour in the time after. The positive sign of the photovoltage is in full agreement

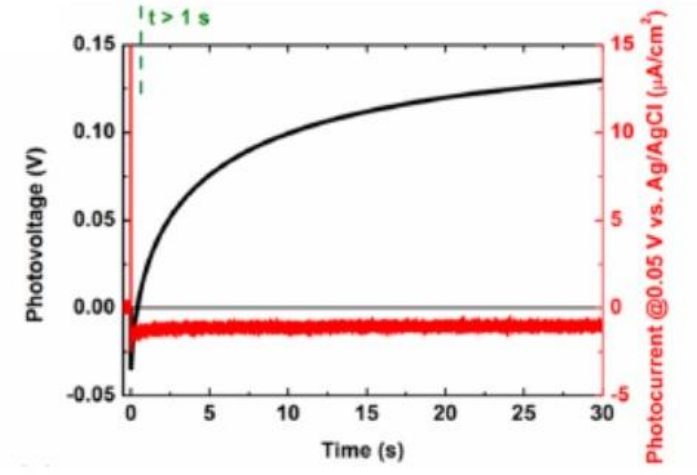

Figure I.6 Photocurrent and photovoltage of P3HT films in water environment. Photovoltage presents two behaviours. First, a capacitive charging, secondly a saturating photovoltage, in agreement with the photocurrent. Therefore, reaction rates are in the range of seconds.

with the MD results, since it is symptomatic of electrons' accumulation at water side of the polymer. The initially negative sign is associated to a capacitive charging of the ITO/P3HT interface, since electrons initially accumulate there. On the other hand, photocurrent is always negative, enhancing a motion of electrons towards the electrolyte: therefore, the motion of electrons described by the photovoltage dynamic generates a net charge-transfer phenomenon, able to reduce oxygen, thus sustaining a faradaic current.

In this picture, the position of the oxygen states should be considered. As shown by the same model, there are free states belonging to oxygen molecules lying in the gap of P3HT: thus, according to the scheme shown in figure I.7, the former presents acceptor sites at the interface. Upon irradiation, different interfacial effects have been reported, depending on the energy of the imping light. UV – light provokes

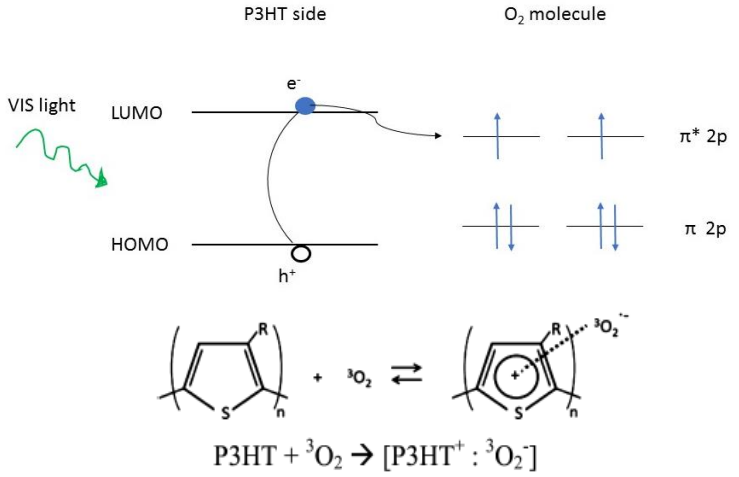

Figure I.7 Polymer vs molecular oxygen levels. Molecular oxygen has two half – filled states, that can react with photogenerated charges of the polymer. One of the possible reactions is the formation of a photodoped complex, shown in the bottom.

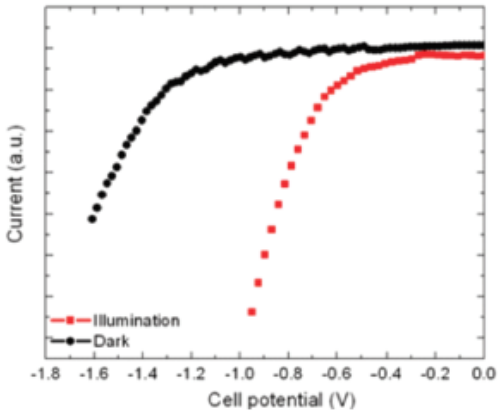

Figure I.8 Current vs potential of P3HT films in water environment. Electron transfer reactions are increased upon illumination (red line) with respect to dark condition (black line).

degradation by radical chain oxidation of the π-electrons, resulting in loss of conjugation and formation of covalent bonding between the carbon and the oxygen. Conversely, visible light irradiation promotes charge transfer reactions between polymer and oxygen, according to figure I.8. This process happens also in dark condition, but it is boosted upon light irradiation (figure I.8, red line): this photodoping generates the formation of a Van der Waals complex located at the surface (figure I.7).

Measures of contact angle (figure I.9) have confirmed this model: it is defined as the angle formed by a drop of liquid on a surface, obtained by considering surface tensions and their minimization. The higher the contact angle, the lower the

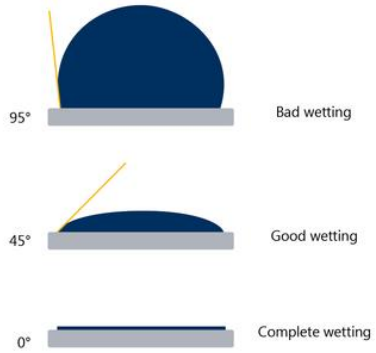

Figure I.9 Contact angle. It gives information about the wettability of a surface. When the contact angle is lower than 90°, the surface is highly hydrophilic. Conversely, for contact angles higher than 90°, the surface is hydrophobic.

hydrophilicity; when we have a hydrophilic surface, the tension exerted by the molecules of the liquid drop is very low, and is said to be wetting the surface. Conversely, hydrophobic surfaces exert a higher tension with the molecules of the liquid, obtaining a bad wetting. The measures of polymer's surface in contact with water upon light irradiation have been compared to the ones in dark condition. The former presents a decrease of the contact angle up to 14% of its dark value: it confirms the hypothesis of photodoped states at the surface, since oxygen induces polarization, reducing the water surface tension. Even if many evidences support the hypothesis of the interaction between oxygen and polymer surface, studies have been worked out to prove what happens in case of oxygen absence [12]. As before, electrochemical measurements have been performed, after previous flux of nitrogen for one hour, obtaining a degassed solution, that has been maintained for the lasting of all the experiments. An I-V characterization shows that the voltage needed for promotion of the reactions has different values depending on light or dark conditions. Quantitively, when the polymer is irradiated, the needed potential is lowered of an amount of 0.6 V. This can be explained taking into account the V_{oc} of the polymer in water environment, that is around 0.35 V: this value seems to be too low to promote the hydrogen evolution, but we should consider that the measured open circuit potential includes also the screening effect due to electrostatic coupling of the ions of the electrolyte at polymer's surface. Therefore, the light speeds up the reaction also in this case; moreover, looking at the energy diagram (figure I.10), and considering the

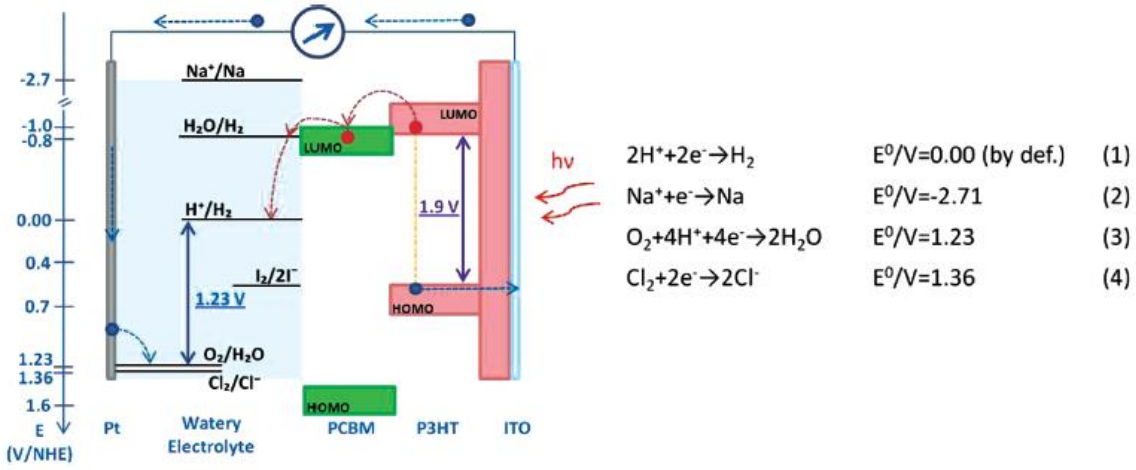

Figure I.10 Energy diagram of possible reactions occurring in the energetic range of P3HT. Looking at the redox potentials, the reactions that can possibly occur are (1) and (3). In this figure, the active region of the device is made of a blend, P3HT:PCBM, used to improve the electron transport.

negative sign of the current, only reductions can be happening at the working electrode site. This means that the only species experiencing a polymer mediated reduction is the couple H^+/H_2, that is hydrogen evolution. At the counter electrode, for kinetic reasons, the oxidation is given by the couple Cl_2/Cl^-. Besides those aspects, having a look at the values of the photocurrent, the hydrogen related one is one order of magnitude lower than the oxygen related one.

I.IV Polymer – H_2O – cells interface

As assessed in the previous chapter, the polymer/electrolyte interface is able to generate a photocurrent, held by different species such as hydrogen or oxygen. Therefore, there is charge accumulation and transfer at the interface: in this view, whatever stays in the electrolytic solution or in contact with the interface itself can be part of those phenomena or can be influenced by them. Previous studies [8], [13] have demonstrated that devices, whose active layer is P3HT or P3HT blends, can be used as optical transducers: the remarkable outcome is that both *in vitro* and *in vivo* models have shown polymer – mediated effects with different device configuration.

In vitro studies have been performed using animal cells: they are grown on the top of the device and their functionalities have been recorded using patch – clamp techniques. In this case, the device is a planar structure, made of a glass slab covered by ITO; on the top of it, both P3HT:PCBM blend and P3HT are spin coated; finally, the device is sterilized and cells are grown on the polymeric film. The experimental evidence shows activation of thermal channels upon polymer photoexcitation. It can be explained considering the deactivation paths of the photogenerated excitons: P3HT

exhibits a low fluorescence yield [14], so recombination of excitons and charges mainly happens by non – radiative pathways. As described in sect. I.II, these involve heat generation after relaxation. This thermal energy is thus released to electrolyte and cells, generating a local increase in temperature.

In vivo studies have been performed with the aim of the *Hydra Vulgaris* animal model (chapter II.V): it is an aquatic polyp able to adhere to a substrate by its foot. In this configuration, only the foot would be in contact with the polymer surface, thus a different approach has been carried out. Works report on stability and reliability of P3HT nanoparticles [9], therefore they have been administered to *hydrae*, being internalized. Now, since the animal is transparent, when it is illuminated, the polymeric nanoparticles have been photoexcited, allowing to study their activity on those animals. Different amazing effects have been reported: first, their behaviour is strongly affected by photoexcited polymer, resulting in an increase of contractions. Second, polymer nanoparticles have shown to strongly increase the expression of *opsin* gene, without the help of prior genetic treatments [15].

Maintaining the approach of the P3HT nanoparticles, the latter have been internalized by the cells, so the polymer surface is in contact with cellular environment. It can be modelled as a solution made of water, Na^+, Cl^-, Ca^{2+} and other ions that maintain a certain osmolality with the external environment. Therefore, it is reasonable to assume reactions to take place mainly with oxygen, being Cl^-/Cl energetically far from polymer's levels. From the nanoparticles point of view, confocal and spectroscopic characterization have been carried out. The former show how nanoparticles are internalized by the cells: being their size of thousands of nanometres, the supposed mechanism is macropinocytosis. Once in the intracellular environment, bigger aggregates of nanoparticles are formed. Despite this, the spectroscopic characterization reports on similar spectra for absorption and PL (chapter II.IV).

I.V Reactive Oxygen Species

Metabolism is the cooperative activity by which the cells obtain energy for living. Multi-enzyme systems cooperate to obtain energy (either by solar energy or by nutrients), polymerize proteins from starting monomeric units (amino acids) and synthetize and biodegrade macromolecules for peculiar cell's functions (membrane lipids, intracellular messengers). Depending on the source of this energy is possible to distinguish among the two main categories of living systems: autotrophs, which can use carbon dioxide, and heterotrophs, which obtain carbon from the environment, i.e. glucose. Thus, metabolism is the sum of all those enzymes catalysed reactions (figure I.11). For those reasons, metabolism can be modelled as a thermodynamic cycle, in

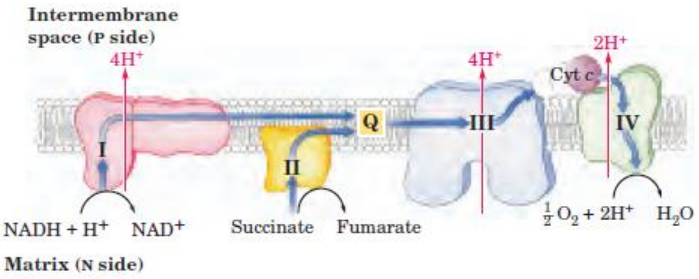

Figure I.11 Steps of the cellular respiration. There are different enzymes and proteins participating in cellular respiration. Mainly, there are four steps in which different proteins are oxidized and reduced. In the last step (IV) cytochrome C participates at superoxide disposal.

which the production of energy is called catabolism and the use of it is called anabolism. Of course, the two are interdependent. Both those processes are made of steps, in which macromolecules as glucose or carbohydrates are disassembled by redox reactions. The final stage is called oxidative phosphorylation, in which the energy of the oxidation drives the synthesis of ATP. It happens into mitochondria, where molecular oxygen is reduced to give water by electron transfer with Nicotinamide Adenine Dinucleotide Phosphate and Flavin Adenine Dinucleotide (NADP and $FADH_2$, respectively). Thus, the respiratory chain can be barely reduced to the following reaction:

$$NADH + H^+ + {}^1/_2\, O_2 \rightarrow NAD^+ + H_2O \qquad (1)$$

All those steps can potentially produce Reactive Oxygen Species (ROS): they chemically come from successive reductions or oxidations of oxygen [16], as shown in the

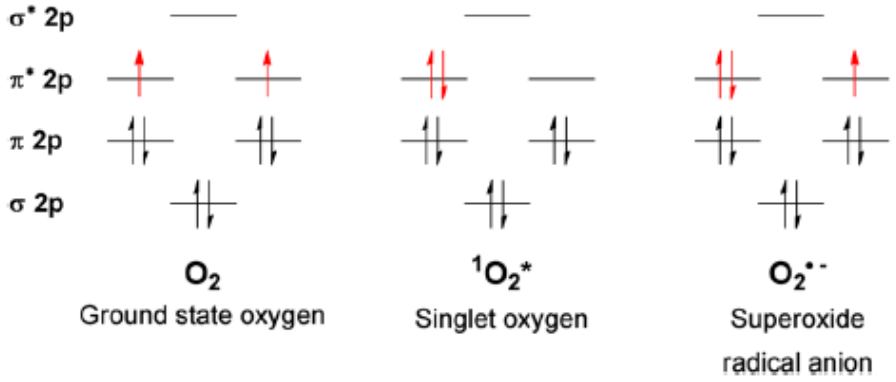

Figure I.12 Successive reductions of molecular oxygen. There are mainly two species related to reduced state of molecular oxygen: singlet oxygen and superoxide. The former has a filled state and an unfilled one: it is more reactive than molecular oxygen since it does not have any spin restriction for the free level. Superoxide radical anion is a highly reactive species, carrying an unpaired electron. Moreover, it carries a negative charge.

figure I.12. The chemistry and the thermodynamics of those species is fundamental for understanding the behaviour and the evolution of this electron transfer. First, we can distinguish among radicals and non-radicals: molecules that present an unpaired electron belong to the former, while those carrying a net charge belong to the latter. To clarify, let us consider some reductions of oxygen (figure I.13). Energy transfer of

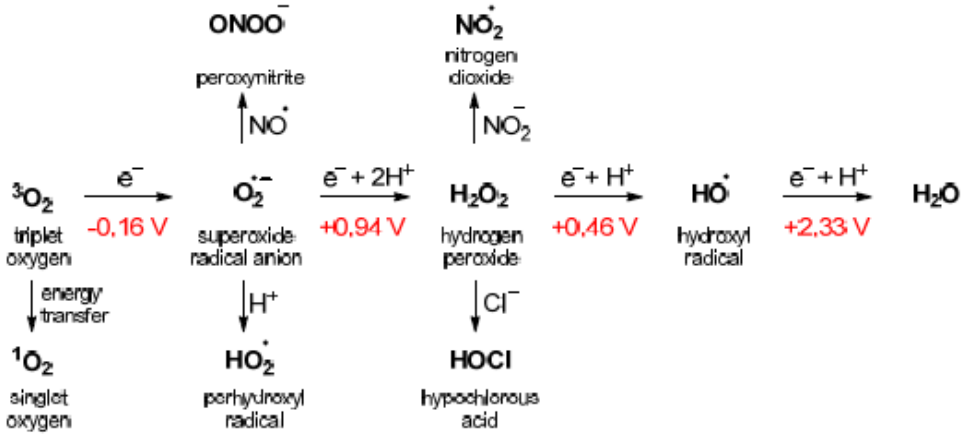

Figure I.13 Energy transfer and electron transfer reactions of molecular oxygen and related redox potential. Focusing on singlet oxygen and superoxide radical anion, the former derives from an energy transfer, while the latter from an electron transfer. Other reductions involve more than one electron, therefore they are less probable than the generation of superoxide.

molecular oxygen results in the generation of singlet oxygen: it carries the same charge of the ground state, but it's more reactive. Both molecular and singlet oxygen can react, but the latter has no spin restriction, while the former does, either: this reflects the strong reactivity of the singlet oxygen rather than molecular one. Electron transfer

(reduction) to both singlet and triplet oxygen leads to superoxide, which carries a negative charge and an unpaired electron. The reactivity of those species is measured by redox potential associated to the reaction: the higher (more positive) the redox potential, the higher the probability of electron transfer. Anyway, external factors such as temperature or pH are able to change the rate constant of reactions. Even if ROS are products of the respiratory chain, they are very dangerous for living systems, since they are able to degrade lipid compounds, thus driving the cell to death [17]. Anyway, they are usually found in living systems, below a certain concentration, that is the physiological level. Current studies have demonstrated their role as second messengers, that is intracellular signalling that triggers functions as proliferation, differentiation and death. Moreover, they influence other messengers, such as Ca^{2+} one, being able to modulate the ionic response of the cell [18].

I.VI Calcium channels

Cells regulate their activity by ions or compounds called second messengers: their changes in concentration are able to trigger many cellular responses [18]. One of those ions is calcium (Ca^{2+}): it is responsible for a variety of cellular functions, such as contraction, secretion, metabolism, gene expression and death [18]. Ca^{2+} is already present in intracellular environment in a concentration of 10^{-7} M, the latter being controlled by calcium pumps and channels located in the endoplasmic reticulum, mitochondria and plasma membrane. External stimuli excite both an influx of Ca^{2+} through Ca^{2+} channels sited in the plasma membrane or a depletion of the ion from the endoplasmic reticulum and mitochondria through calcium pumps, in both cases achieving a change in the concentration of cytosolic Ca^{2+}. Commonly, Ca^{2+} activity is not barely related to a single spike of increase or decrease in concentration, instead, it is associated to an oscillatory behaviour, whose period can last for few seconds, even for a constant external stimulus. It has been associated to a feedback regulatory activity of Ca^{2+} channels [19]. There are two actions related to Ca^{2+}, one of which is the ability of binding and unbinding to proteins; for example, Calmodulin is a protein whose Ca^{2+} - bound state triggers changes in the conformation of other proteins, like troponin, responsible for muscular contractions. The other influence of Ca^{2+} on cellular activity is its charge movement, able to change the membrane potential in the form of calcium current. An example of this kind of regulation comes from vision cascade: absorption of photons by cones and rods triggers the secretion of cGMP, a protein whose increase in concentration regulates ion fluxes, thus the polarization of the

membrane potential. The latter, when dealing with excitable cells, generates an action potential, i.e. a decrease and subsequent increase in the polarization of cellular membrane, that initiates communications between neurons. Therefore, Ca^{2+} activity is studied whenever cellular functions need to be detected. There are many experimental methods to monitor Ca^{2+} activity, such as imaging and patch – clamp techniques: the formers are widely used, based on the activation of a compound that becomes fluorescent when binds Ca^{2+}. When Ca^{2+} dynamic is triggered, a peak in the fluorescence of the probe is recorded. The patch – clamp technique measures the voltage drop across the membrane, but it is related to different ions. For isolating the drop due to Ca^{2+} homeostasis, is necessary to silence all the other ion – dependent channels. Thus, pre – treatment of the cell is mandatory.

There are many evidences in literature about the mutual interplay between Ca^{2+} and ROS. The cross – talk is related to Ca^{2+} modulated ROS production and to ROS modulated Ca^{2+} signalling. Ca^{2+} promotes energy production during Krebs cycle, being able to modify the metabolic state of the cell: the increase of the latter results in an increased respiratory chain electron leakage and subsequent increase in ROS levels [20]. Changes in ROS concentration may both lead to increase or decrease in Ca^{2+} concentration: the former is induced by ROS stimulation of kinase, while the latter is related to direct oxidation of Ca^{2+} channel by ROS. Moreover, differences in the generated species, amount and timing can contribute to variable effects on Ca^{2+} channels. There are many on – going studies trying to explain all the possible mechanisms involving a cross talk between ROS and Ca^{2+}.

II. Methods

In this section, an in-depth description of materials and experimental methods is provided. ROS detection is based on fluorescence imaging methods. To detect intracellular Reactive Oxygen Species (ROS) we employ three different kinds of molecular probes. Since they are supposed to be used upon light, we carry out a characterization study of their stability properties. Main optical and spectroscopic properties of photoactive polymer nanoparticles, as well as information about their biocompatibility, is provided. Finally, cell culturing techniques and handling and maintenance procedure of the Hydra in vivo model are provided.

II.I Imaging

Imaging techniques are the most suitable for many reasons: first, their signal can be directly compared to the amount of oxidized probe, corresponding to the generated ROS. Second, by stacking images, is possible to check whether fluorescence increases correspond to the position of the nanoparticles inside the cell. Fluorescence measurements are carried out by using an inverted microscope (Nikon, Eclipse Ti – S) coupled with LED light sources (Lumencor, SpectraX), to provide excitation in different regions of the visible spectrum.

Figure II.1 presents the scheme of the imaging setup. The emission of the specimen passes through the beam splitter and the emission filter, finally hitting onto the detector. The excitation is provided by an array of three independent solid state

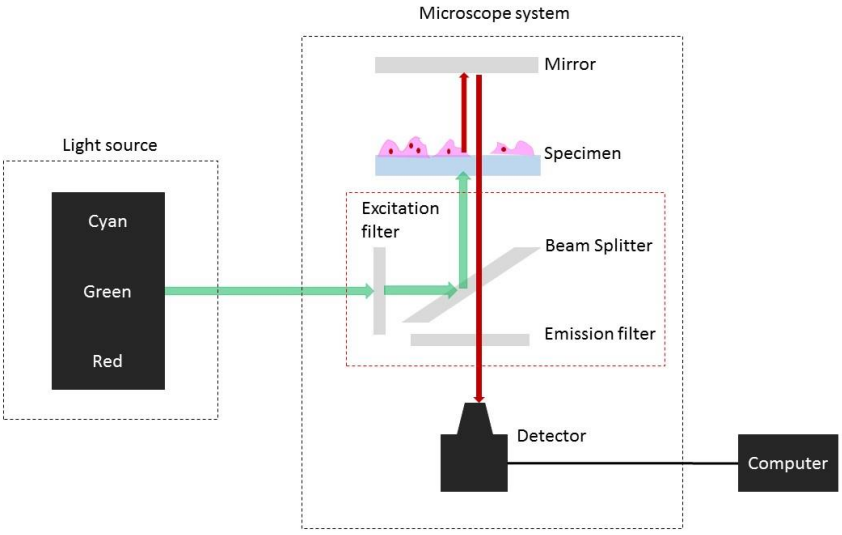

Figure II.1 Scheme of the imaging setup. The figure presents the scheme of the imaging setup: a filtering system decouples the excitation from the emission.

light sources, coupled to the microscope by optical fibres and collimator system. Even if they are filtered before entering the microscope, their emission spectra are broad (figure II.2).

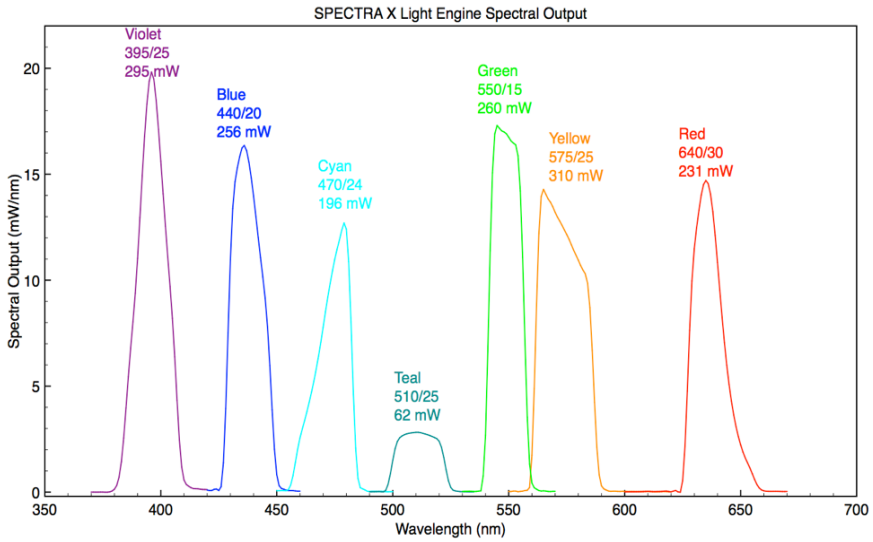

Figure II.2 Emission spectra of the LED sources coupled to the imaging setup. Our setup is equipped with blue, cyan, green and red LEDs. Their spectra are broad, therefore another filtering system is added.

That's why an additional filtering system is necessary before reaching the specimen. Filters are contained in the red box in figure II.1. The latter is constituted of a rotating disk, where different filters are incorporated at different positions. Their spectral characteristics are reported in the table II.1.

Table II.1 Excitation and emission ranges for the imaging setup.

Filter	Excitation	Emission
FITC (Nikon)	465 – 495 nm	515 – 555 nm
TRITC (Nikon)	540 ± 25 nm	605 ± 55 nm

The microscope provides bright field and fluorescence images (figure II.3, left and right side respectively). In both cases is straightforward to distinguish each cell.

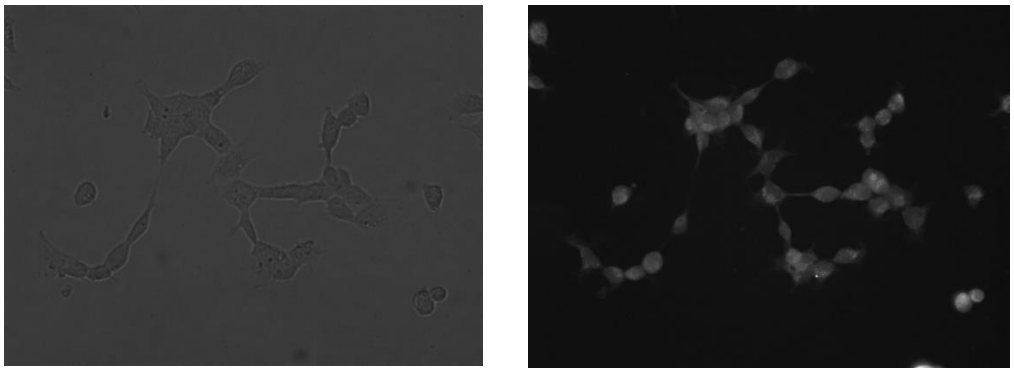

Figure II.3 Images taken at the microscope. (Left) Bright filed image showing HEK cells. (Right) Fluoresce image of the same region of the bright field. The fluorescence is the response of a molecular probe for Reactive oxygen species.

Immediately after the beam splitter, there is a rotating module related to the zoom selection: there are three possibilities, 4x, 20x, 40x. Each of them provides a different spot size, so a different illumination power density, reported in table II.2. Moreover, the illuminated area selects the number of cells that will be examined: thus, 4x zoom will provide a big number of cells, but a very low power density, while 40x one provides just a few cells and a higher power density. For our purposes, the best trade-off is given by 20x zoom unit, since it gives the right power density and a number of cells ranging between 20 and 100. This is crucial for the statistical standing of the experiments.

Table II.2 Illuminated area and related powers of the imaging system.

Zoom	Area	Power density (λ = 550nm)
4x	23 mm^2	2.17 mW/ mm^2
20x	0.92 mm^2	54.34 mW/ mm^2
40x	0.23 mm^2	217.39 mW/ mm^2

Images are acquired by a CCD camera (Photometrics, Coolsnap MYO), whose parameters can be controlled by NIS – elements software (Nikon). The parameter of interest is the integration time. It is the time over which the shutter of the camera is open, thus it determines the number of photons hitting the detector. It ranges from 10 ms up to few seconds. For constant source power, high fluorescence yields require low integration time. The opposite holds for low fluorescence yields. Experiments with H_2DCFDA present a high fluorescent yield, while APF and HPF

Table II.3 Integration time and power density for the three probes.

Probe	Integration Time	Power density
H_2DCFDA	300 ms	5 mW/mm^2
APF	500 ms	12.24 mW/mm^2
HPF	500 ms	12.24 mW/mm^2

require higher integration time (see table II.3 for details). Looking at the absorption spectra of the probes (chapter II.II), the best matching LED for excitation is the cyan one (470 ± 24 nm). The power of the LED is strictly related to the amount of fluorescence. Anyway, especially experiments with H_2DCFDA require low power densities, to avoid its auto – oxidation. Both power of LEDs and integration times for the different probes are reported in the table below.

Image analysis has been performed with ImageJ software. A region of interest (ROI) is set on each cell's cytoplasm and another one is set in a region where there are no cells, to evaluate the background contribution. For each pixel contained in the ROI, the software gives back a number ranging from 0 to 255, the lower value corresponding to zero fluorescence, 255 being detector's saturation. Since each ROI contains more than one pixel, ImageJ gives a value averaged over all the pixels contained in the ROI. At this point we end up with a number of data equal to the number of the cells. Then, background is subtracted from each value. Finally, all data are mediated. Medium values are reported with the standard error.

II.II Molecular probes for Reactive Oxygen Species

ROS can be detected either by electrochemical or by optical methods. The former is based on specific reactions between a ROS species and a proper electrode, whose electrochemical potential toward the considered species is known. Upon proper calibration of the system, production of ROS species is detected by chrono-amperometry measurements. Imaging techniques are based on chemical reactions between a probe molecule and the targeted ROS. The probe shows a change in its fluorescence spectrum (either in intensity or in the emission peak position) upon oxidation by the ROS. Measurement of the probe emission provides a direct information about the presence of ROS. Fluorescence imaging methods are by far the most widely diffused and accepted methods in biology, for several reasons: they provide a direct information of the intracellular ROS production; they are easily coupled to in vitro cell cultures; many probes are commercially available. Both ratiometric and non-ratiometric probes are currently available. Both are constituted by a molecule that can be internalized within the cell membrane. In the first case, however, the molecule does not exhibit fluorescence until it reacts with a ROS. The intensity of fluorescence is a clear, though qualitative signature of intracellular ROS production. In the case of ratiometric probes, a fluorescent molecule is used, which exhibits a change in its fluorescence peak position/relative weight respect to secondary emission peaks in the presence of ROS. Thus, the bigger the shift, the higher the concentration of ROS; this kind of measure allows to quantitatively evaluate the number of moles of generated ROS.

Many different probes are commercially available, mainly classified according to their ROS selectivity and detection efficiency. There are ones sensitive to superoxide

or to singlet oxygen for example, but there are also less specific ones that exhibit sensitivity to a number of different species with different relative efficiencies. In this work, 5-(and-6)-carboxy-2',7'-dichlorodihydrofluorescein diacetate (H_2DCFDA, Thermofisher), 2-[6-(4V-Hydroxy) phenoxy-3H-xanthen-3-on-9-yl]benzoic acid (APF, Thermofisher) and 2-[6-(4V-amino) phenoxy-3H-xanthen-3-on-9-yl] benzoic acid (HPF, Thermofisher) were used, in order to gain and combine information about the production of different species.

H_2DCFDA is a non-fluorescent compound: its oxidation generates a fluorescence peak in the green region (ex/em = 498/522, figure II.4). This probe was initially thought to be a specific indicator for H_2O_2, but later on it has been demonstrated that it can be oxidized also by other ROS, such as HO·. H_2DCFDA

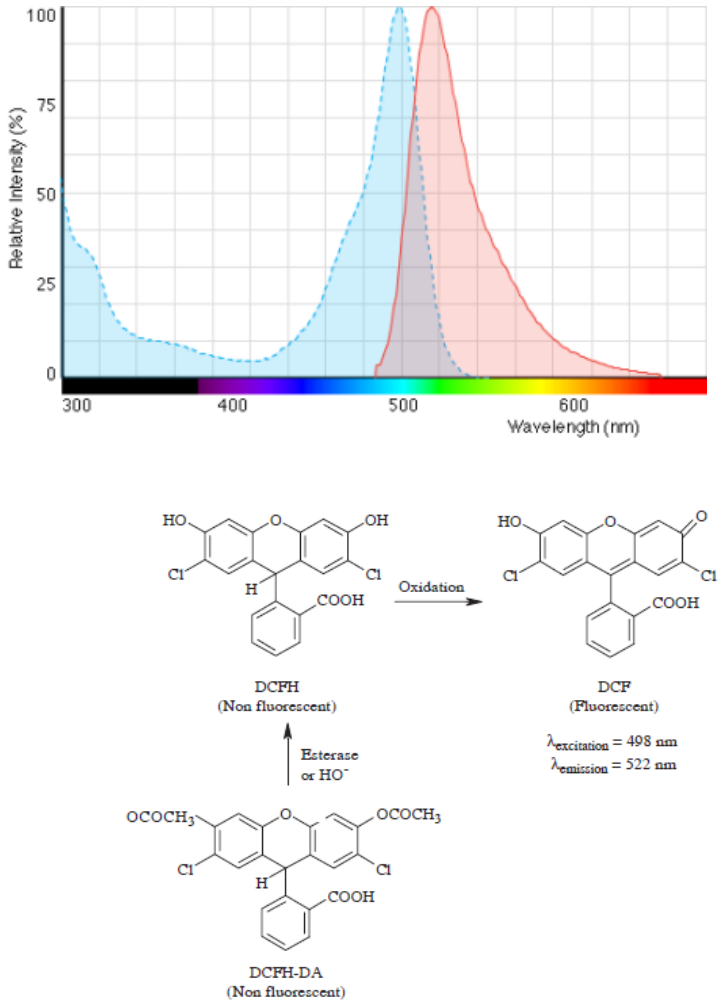

Figure II.4 Spectral characteristics of H_2DCFDA. The absorption (blue) and emission (red) spectra of the probe are shown. The bottom part shows the esterase that the probe undergoes within the oxidation. Is worth noting that the probe becomes fluorescent only after oxidation reaction.

penetrates the cell membrane, undergoing rapid hydrolysation through a process called esterase. The result is a not-fluorescent compound, which however exhibits

strong emission upon oxidation. The cytosol internalization capability gives specificity to the probe to internal ROS generation. Unfortunately, this compound is highly light sensitive [21]. The stock solution has been diluted in extracellular medium (KRH) at a final concentration of 25 µM. Cells are incubated for 30 minutes at room temperature and ambient light condition. Then, three washes with KRH are performed, to remove the excess product.

HPF and APF are non-fluorescent derivatives of fluorescein. Their reaction with ROS provokes the dearylation of the oxygen (shown in figure II.5) that leads to a strong fluorescence in the green region. Setsukinai et al [22] studied the reactivity and the selectivity of these probes, showing their selectivity to HO· generated by Fenton reaction (figure II.5). Notably, APF is mainly sensitive to HOCl, while HPF is not. Moreover, at variance with DCF, they are not prone to self-oxidation, and can be used both in cellular and enzymatic systems. Upon bounding with ROS, those probes exhibit an absorption peak at 490 nm, to which corresponds an emission at 515 nm (spectra are shown in figure II.6, APF on the left and HPF on the right). The stock solution is diluted in extracellular medium (KRH) up to a final concentration of 5 µM and

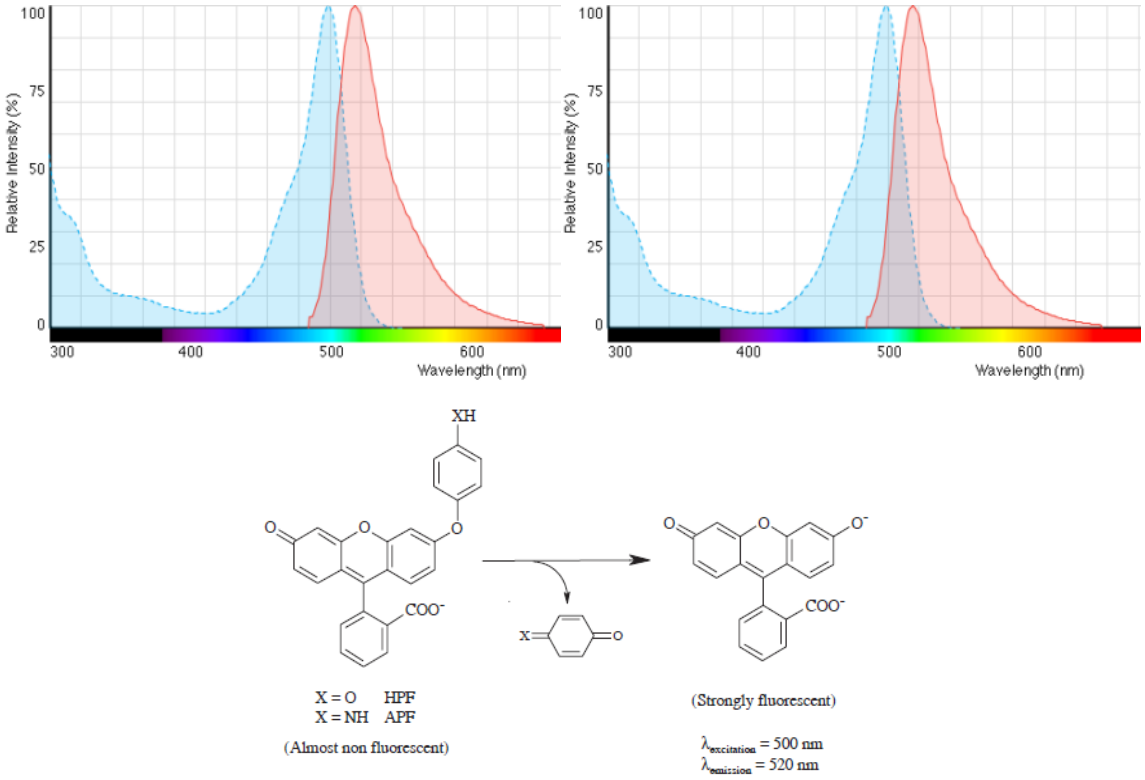

Figure II.5 Spectral characteristics of APF (left) and HPF (right). The absorption (blue) and emission (red) spectra of the probe are shown. The bottom part shows the esterase that the probe undergoes within the oxidation. Is worth noting that the probe becomes fluorescent only after oxidation reaction.

administered to the cells. The incubation lasts for 40 minutes at room temperature and ambient light. Then, cells are washed with KRH to get rid of the excess product.

Stimulation of the nanoparticles is obtained by illumination with green LED (λ_{em} = 540 nm). Looking at the data reported in chapter II.I, the emission of the probe overlaps with the absorption of the nanoparticles. Therefore, fluorescence of the probe can be affected. Moreover, the emission of the nanoparticle can affect the measurements. For this reasons, imaging has been performed using the FITC filter: its cut off is at 515 – 555 nm, therefore the emission of the nanoparticles is cut. The probes are easily oxidized when illuminated, therefore is added at the end of the illumination time.

The probes give a snapshot of the moment at which we are looking at. Fluorescence is giving the amount of ROS that are present when the probe has been internalized by the cell. So, the best would be to measure the fluorescence of the probe during the illumination of the nanoparticles. Anyway, probes are very sensitive to light degradation, thus they cannot be directly illuminated. For overcoming this problem, optical stimulation is performed in cells' medium without the probe; the latter is added at the end of the illumination. Depending on the sample, different concentrations and incubation time are required. The table II.4 summarizes both those quantities both for *hydra vulgaris hydra vulgaris* and for HEK cells.

Table II.4 Concentrations of molecular probes both for hydra vulgaris and HEK cells.

Probe	Hydra Vulgaris	HEK cells
H_2DCF-DA	15 minutes, 25 µM	30 minutes, 25 µM
HPF	1 hour, 10 µM	40 minutes, 5 µM
APF	1 hour, 10 µM	40 minutes, 5 µM

II.III Ca^{2+} imaging

There are many ways to investigate Ca^{2+} production by cells: some of them provide the analysis of the membrane potential, being Ca^{2+} responsible for ionic concentration changes. Others provide molecular compounds that bind Ca^{2+} ions in the intracellular environment, becoming fluorescent. The former requires patch – clamp technique, by which is possible to measure both current and voltage drop on the plasma membrane. This measure is affected by other ionic currents, as K^+ and Na^+ ones, thus silencing of those ions is necessary for isolating only Ca^{2+} effects. Conversely, imaging techniques are easier to be performed, being the fluorophore selective to Ca^{2+} ions. Still holds the difference between ratiometric and non – ratiometric ones, only the latter being quantitative. In this work, Fluo – 4 AM (Thermofisher, molecular structure given in figure on the left) has been used as calcium

indicator. It is a cellular permeant compound, whose chemical formula is reported in figure II.6. The esterification of the ester groups allows membrane permeation, giving a fluorescent compound located in the intracellular environment. The fluorescent compound exhibits an absorption peak at 485 nm and the corresponding emission at 520 nm, as reported in figure II.6. The mother solution has been diluted in extracellular medium (KRH) up to a final concentration of 1 µM. Incubation lasts 20 minutes at 37 °C and 5% of CO_2. Then, cells are washed for 10 minutes in extracellular solution. The

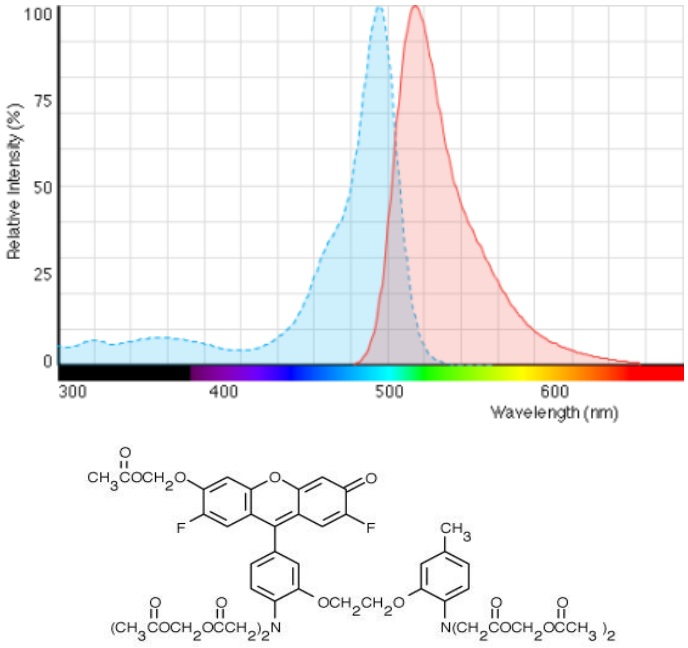

Figure II.6 Spectral characteristics of Ca^{2+} indicator (Fluo – 4). The absorption (blue) and emission (red) spectra of the probe are shown. The molecular structure is presented at the bottom.

measured variations are related to internal Ca^{2+} dynamics, but the ion can be internalized from the extracellular solution or can be released by inner compartments, as mitochondria or endoplasmic reticulum. To distinguish between these two activities, we used two different extracellular solutions, KRH and KRH calcium free. These solutions are used during the measurements. Dynamics recorded with KRH give information on Ca^{2+} homeostasis dependent on internalization, while those recorded with KRH Ca^{2+} free are related only to intracellular Ca^{2+} releases. Ca^{2+} dynamics present a rising and a falling profile that relax to the basal level during the stimulation. Therefore, Ca^{2+} dynamics must be recorded in real time: cells treated with P3HT – NPs should be illuminated with green light while recording the response of the Fluo4. Figure II.7 shows the scheme for carrying out this measure with the setup described in methods (chapter II.I). The detector is not able to separate the green light coming from the excited probe and the one coming from the one used to excite the nanoparticles. Since P3HT – NPs present a broad absorption spectrum, cyan led too can excite the nanoparticles at high power densities. Thus, the measurements are performed with

low (P = 34,78 mW/mm^2) and high (P = 247,82 mW/mm^2) power densities; the illumination lasts for 3 minutes. The emission is recorded with the FITC filter, so that the emission of the nanoparticles is cut.

Ca^{2+} waves are connected to ROS modulation. A straightforward way to verify

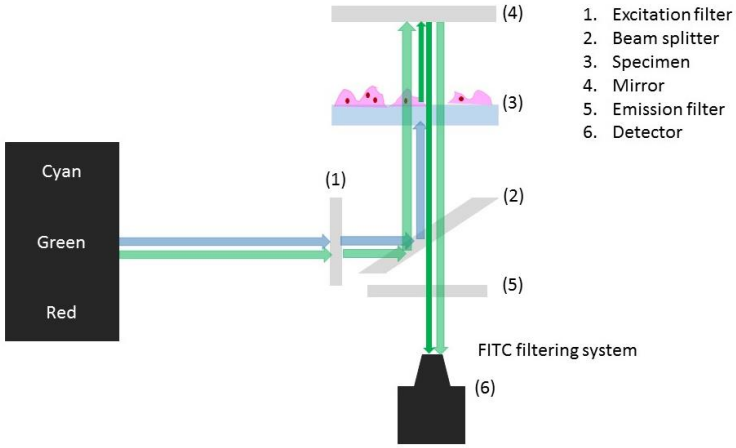

Figure II.7 Ca^{2+} imaging setup scheme. The image shows what happens using also the green excitation: the filtering system let it pass, therefore the detector collects both the emission of the probe and the excitation light. For this reason, cyan LED is used both for excitation of the nanoparticles and of the probe.

this connection is to inhibit ROS production and measure Ca^{2+} waves. N – acetyl – cysteine (NAC) is an ordinary ROS inhibitor [23], since radical species easily reduce the double bond. Therefore, cells are incubated with Fluo4 for 20 minutes as in the previous case, then the 10 minutes' wash is done in a bath of NAC 5mM diluted in KRH. The same solution has been used during the measurement.

II.IV Nanoparticles characterization

CP – NPs are synthetized in colloidal form, that is a co – existance of liquid and almost solid phase. A colloidal phase is defined to be stable when the two immiscible phases do not separate. Therefore, the stability is determined by ionic forces acting between the surface of the nanoparticle and the solvent's components. Usually, the solvent contains ions and the nanoparticles possesses a charge: for this reason, as soon as the colloidal phase is reached, there will be a shield effect of opposite charged ions (Stern layer, see figure II.8). Within this range, the ions are adsorbed by the

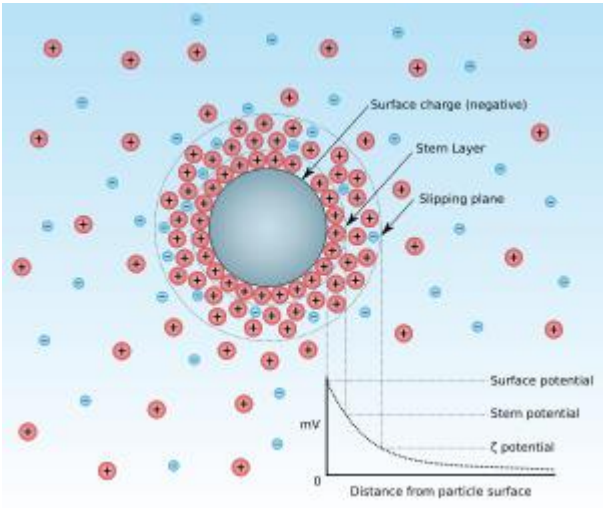

Figure II.8 Scheme of Z - potential identification. The Z – potential is related to the electrostatic stability of the probe, since it depends on the surface charge of the nanoparticle itself.

nanoparticle surface. This generates a charge that has to be compensated: it happens within the slipping plane, where charges feel the Coulomb attraction with the previous layer. This double-layer of charges provokes a potential drop, called Z-potential. Now, thinking at having a huge number of nanoparticles in suspension, the higher their repulsion, the lower the aggregation. Thus, the Z-potential is directly linked to colloidal stability (table II.5): a high Z-potential reflects a high repulsion, so nanoparticles are not aggregating, while a low Z-potential allows nanoparticles aggregation. The latter

Table II.5 Colloidal stability related to Z – potential.

Z – potential (mV)	Stability of the colloid
0 ÷±5	Rapid coagulation, flocculation
±10 ÷±30	Incipient stability
±30 ÷±40	Moderate stability
±40 ÷±60*	Good stability
≥±61	Excellent stability

destroys the colloidal phase. For P3HT nanoparticles (P3HT-NPs), the measured Z-potential is around -36 mV, so falls in the range of good stability. The radius is a statistical variable, since available synthesis techniques do not control it. This heterogeneity is measured by the polydispersity index, that is the variance of the radius weighted over the molecular weight. Common values for good colloidal solutions are around 0.1.

The fabrication of nanoparticles follows different synthetic methods, usually based on hydrophobicity/hydrophilicity of the material of the nanoparticles itself with the solvent. Moreover, for our purpose, the process should be performed in sterile conditions, since the nanoparticles will be injected in living systems. After many attempts, the best procedure was the re-precipitation [9], consisting of two phases (figure II.9).

- Phase 1: solution of P3HT (obtained by oxidative polymerization of P3HT with ferric chloride [15]) is stirred in water, where nanoparticles are formed within few seconds, thanks to different hydrophilicity of all the participants;
- Phase 2: different centrifugation speeds and durations separate bigger and smaller nanoparticles.

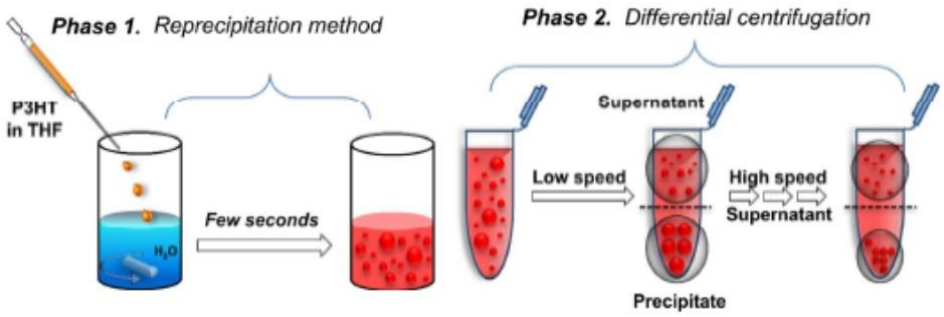

Figure II.9 Phases of P3HT - NPs fabrication. Phase 1 consists in making the polymer molecules aggregating, forming the nanoparticles, as a consequence of the bad solvent in which they are put. This method forms nanoparticles of different size. Phase 2 separates these sizes using different centrifugation speeds.

Both phases can be performed under sterile hood, thus the nanoparticles are sterile, too. This characteristic is mandatory when dealing with cells. P3HT – NPs used for the experiments presented here, have a radius of 237 nm with a polydispersity index of 0.12.

P3HT-NPs are then optically characterized, so their UV-VIS absorption and continuous-wave photoluminescence (CW-PL) have been reported (figure II.10). Two

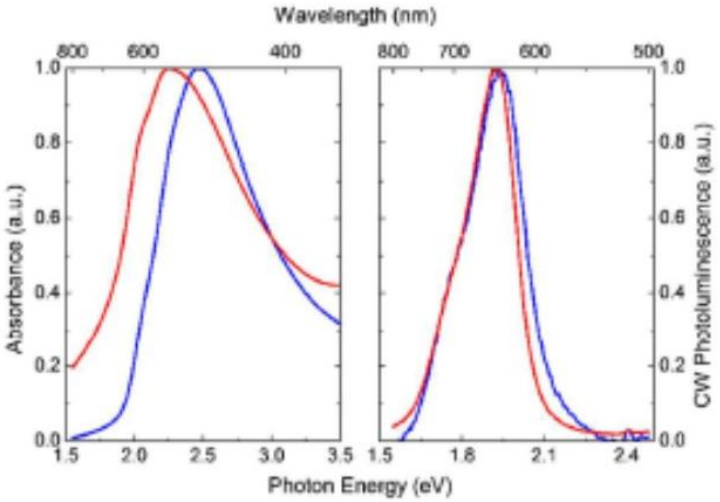

Figure II.10 Absorbance and CW photoluminescence of P3HT - NPs, Data are reported for two different nanoparticle dimensions, r_{red} = 344 nm, r_{blue} = 148 nm. The dimension affect the absorbance, provoking a shift towards higher wavelength with the increase of the radius.

different sizes of nanoparticles (148 nm-sized in blue, 344 nm-sized in red) are shown. The size of nanoparticles affects the absorbance, while the emission is not affected, either. Moreover, the optical characteristic of film and suspension of P3HT are compared, giving information about the effects of aggregates. The formation of the latter provokes a red shift, probably related to the different screening ability of the two geometries and so to a change in conformation. This has to be taken into account, since nanoparticles in the cell environment present aggregates. Moreover, SEM images (figure II.11) show the shape of the surface. The lower the roughness the higher the stability.

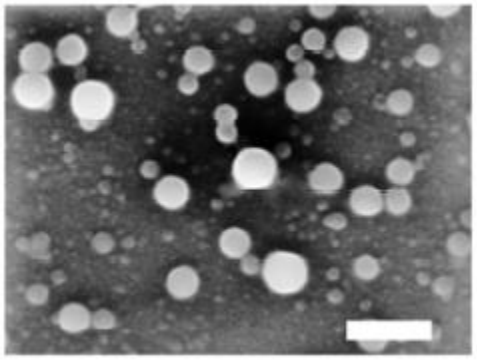

Figure II.11 SEM image of P3HT - NPs. SEM image gives information about the roughness. The surface of these nanoparticles is smooth, indicating a good stability.

P3HT-NPs' biocompatibility is a crucial issue, since the aim is to inject them into human tissues. It can be verified by MTT assay or by Ca^{2+} imaging. The former is a colorimetric method, while the latter is a fluorometric one, both associated to cell

viability. MTT measures enzymatic activity of mitochondria, while Ca^{2+} imaging measures the activity of ion channels of the cell. For both cases, the P3HT-NPs demonstrated to be non-toxic. Confocal images show their internalization, that usually happens within few minutes [9].

Spectroscopic measurements performed on nanoparticles internalized by the cell are provided. Cytoplasm presents different dielectric and ionic features with respect to extracellular environment and water. Thus, the spectroscopic features of P3HT – NPs can be affected. Time-resolved fluorescence provides information about [9] decay rates and relaxation dynamics (figure II.12). Fluorescence of nanoparticles inside water and extracellular environment (grey, blue, red lines) has been compared with the one inside the cell (green lines). The interaction with the cytoplasm provokes

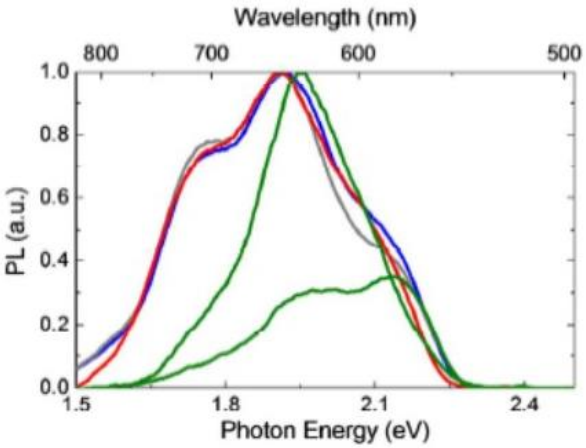

Figure II.12 PL of P3HT – NPs. Grey: PL of nanoparticles in water. **Blue**: PL of nanoparticles in extracellular solution (KRH). **Red**: Gaussian fit of the previous. **Green**: PL of nanoparticles inside the cell. Cellular environment provokes the disappearance of the shoulder at lower energy, attributed to the formation of the aggregates.

the disappearing of the peak at low energy (E = 1.7 eV), while remains the shoulder at higher energies (E = 2.2 eV). The main peak at E = 1.9 eV results to be unaffected. Inside the cell, nanoparticles show higher aggregation with respect to solution's ones: the latter present a peak at lower energy probably due to free chains, that disappears when they aggregate. Moreover, is not possible to exclude interactions with the cytoplasm or with plasma membrane: endocytosis' vesicles can reduce the degrees of freedom of external free chains, resulting in the loss of the lower shoulder.

Pump – probe spectroscopy measurements in the energy range of visible light show an excitation that deactivates in a few picoseconds. Moreover, figure II.13 shows a comparison between the lifetime of the excited states in the cell (green line) and in

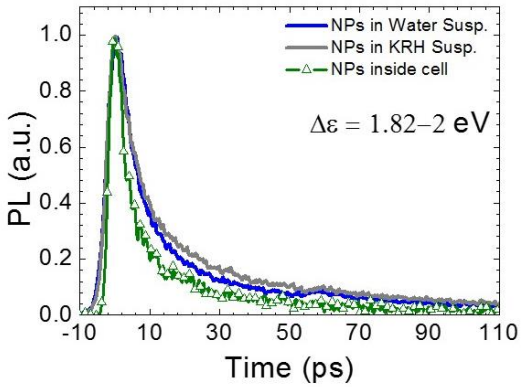

Figure II.13 Time - resolved PL of P3HT - NPs. Blue: PL of nanoparticles in water suspension. **Grey**: PL of nanoparticles in KRH. **Green**: PL of nanoparticles in the cells. Cellular environment affects the PL, decreasing the lifetime of the generated states.

water (blue line), depicting a shorter lifetime in the first case. To ensure that the extracellular fluid (KRH) is not affecting the measure, pump – probe is reported also for nanoparticles dispersed in this medium, grey line. Nanoparticles in KRH suspension show a higher lifetime with respect to cellular environment. A reasonable explanation for this behaviour is the high intensity of the pump source: it excites the system up to high energy states with a deactivation path faster than less energetic ones. This hypothesis is still under studies. Figure II.14 presents an analysis over longer lifetimes.

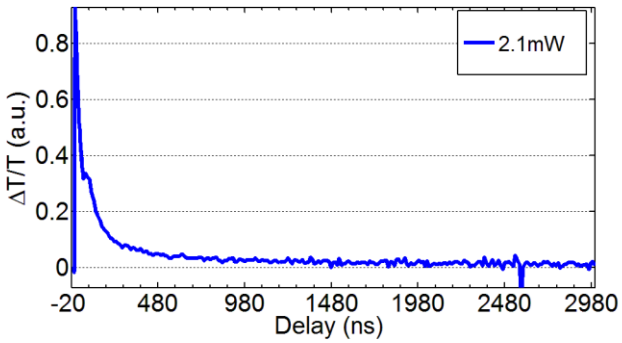

Figure II.14 Pump - probe temporal analysis.

It shows a small amount of charges living up to hundreds of nanoseconds, favouring the hypothesis of long living states. The effects of charge generation are mainly related to electron transfer reactions with species in solution, such as oxygen.

II.V Electrochemical measurement

Electrochemical measurement represents a quantitative procedure for calculating the current related to P3HT – NPs. Common working electrodes present sensitivity to different species (see appendix B), but a functionalization of the surface provides a high selectivity for ionic species in the solution. WE has been functionalized following some steps, reported in figure II.15. First, a thin film of Au of 80 nm of thickness is evaporated on a glass substrate. Then, they are washed with cycles of water, acetone and isopropanol. These gold electrodes (200x150 mm) are then put in a solution of N – Acetyl – Cysteine 2 mM in phosphate buffer 10 mM (pH = 7) for two hours. The high affinity of gold with thiol groups provides the binding of the cysteine to the electrode surface. A copious wash in water is performed after this step. Then, this electrode is incubated in a 10% w/V solution of 1 – ethyl – 3 – (3 – dimethylaminopropyl) carbodiimide (EDC) in water, lasting 2 hours at 25 °C. Within

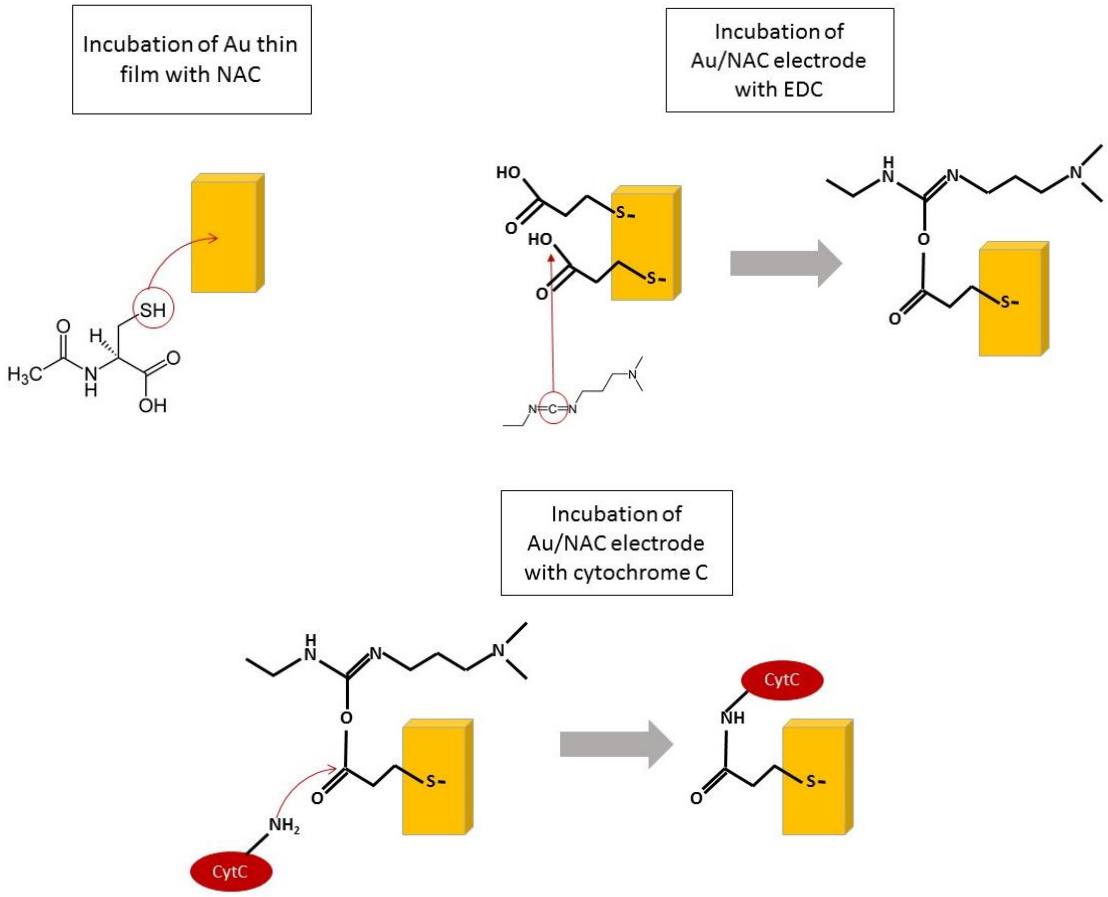

Figure II.15 Steps of working electrode functionalization with cytochrome C. In the first step, the thiol groups of the NAC bound the Au electrode, forming a highly hydrophilic surface. The incubation with the EDC (second step) generates neutrophilic sites for creating ester bonds. Third step regards the incubation with cytochrome C: the amine group of the peptides that cover the Haem group of the protein are able to link the ester bond. Therefore, the cytochrome C is covalently attached to the gold electrode.

this passage, a neutrophilic site in the ester bond is created: is the site where cytochrome will link. The electrodes are again washed in water. Electrodes are finally incubated in a solution of cytochrome C (4.2 g/L in 10 mM phosphate buffer, pH = 7) at 4 °C for 6 hours. The amine group of the cytochrome C, located in the peptides all around, will attach the carbon of the ester group, releasing the upper chain of figure II.16. An exhaustive wash with 10 mM phosphate buffer [24] allows to eliminate all these chains from the electrode, being water soluble.

The three electrodes are usually kept in the same cell. In order to avoid nanoparticles contamination of the platinum wire counter electrode (CE) and of the Ag/AgCl wire reference electrode (RE), the latter are taken in a compartment different from the one of the WE. The two compartments are ionically linked by a salt bridge. Figure II.16 reports the scheme of the setup. Current is measured by Autolab potentiostat coupled with Nova 1.10 software. Light source is made of a blue LED

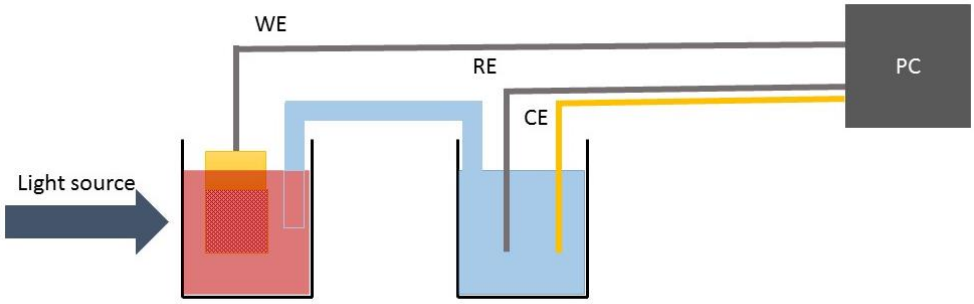

Figure II.16 Electrochemical measurement's setup. The two Becher are connected by a saline bridge. Reference and counter electrode are kept in a separate Becher to avoid contaminations.

(ThorLabs) exhibiting a power of 2,78 mW/mm^2. Measures are then analysed with Origin 8.1. Cyclic voltammetry is carried out by forcing an external potential in a range (-0,6 V; 0,3 V) and measuring the generated current. These measures are necessary for individuating the oxidation and reduction potential of cytochrome C in our system. This because the potentials are affected both by environmental conditions, such as temperature, and by the chosen electrodes. In our case, they are wires of platinum and AgCl. Figure II.17 reports on the voltammetry in dark condition for a solution of 4,2 g/L of cytochrome dissolved in 10 mM phosphate buffer. This measure is carried out with the Au/NAC working electrode. The activity of the cytochrome is the same of

the reported one [24]. Thus, the reduction potential is V_{red} = -0.044 V while the oxidation one is V_{ox} = -0.026 V.

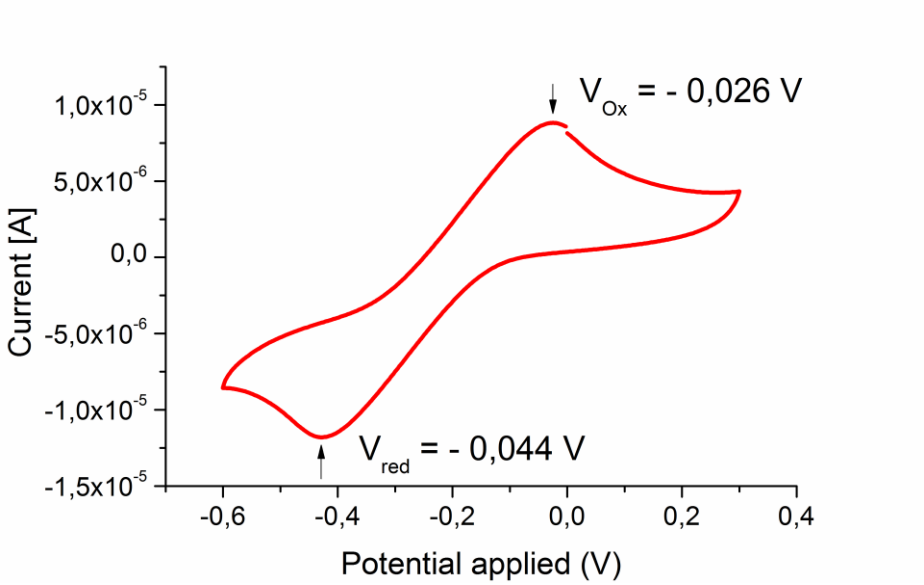

Figure II.17 Cyclic voltammetry of cytochrome C in phosphate buffer. The cyclic voltammetry is measured referring to Au electrode. The oxidation and reduction potential of the cytochrome C are highlighted in figure.

Chronoamperometry consists in measuring the current generated at a fixed external potential (Appendix B). The illumination pattern is 200 s dark, 600 s light, 200 s dark, for a total measure duration of 1000 s. The first 200 s are necessary to let the system relax when the external potential is applied. The latter 200 s are necessary for relaxing the system after the illumination. The power density is 2,78 mW/mm^2, at a central wavelength of 470 nm. This measure is carried out both at the oxidation and at the reduction potential of the cytochrome C. The former forces the immobilized cytochrome C to lose its electron. Therefore, whenever the superoxide binds the cytochrome, the external potential forces the latter to lose the acquired electron. In this way, there are always sites for receiving the electron of the superoxide on the WE.

II.VI Cells' culture

There are many commercially available cell lines, being different for species and characteristic. The cells used for this work are Human Embryonic Kidney (HEK) 293 cells. They have been isolated from the kidney of an embryo in 1973 (van der Eb laboratories, Leiden, The Netherlands) and have been genetically modified to be immortal. In this way, the same vial is ideally able to give cells for ever, thus avoiding any sacrifice of animals. They present ease of handling and capacity of growth on different substrates. For all those reasons, they are the best choice for studying the

reactions occurring at the interface of our hybrid system. Is worth noting that the results obtained with HEK cells are not easily transferred to more complex cells, like neurons. This because the membrane is slightly different and so all the electrophysiological properties. Anyway, they present a good compromise for understanding the basic mechanism and biophysics happening at the hybrid interface.

Glass substrates are cleaned by sonication (10 minutes in ultrapure water, 10 minutes in acetone, 10 minutes in isopropanol), to eliminate dust and other chemical residuals. Then, they are put in oven at 120 °C for two hours. From now on, they are sterile and so they should be handled only under biological hood. The glass substrates are put in a bath of fibronectin (Thermofisher) diluted in Krebs-Ringers Henseleit solution (KRH, for doses and preparation, see appendix C) at a final concentration of 2 µg/ml. This incubation lasts for 30 minutes at 37 °C. Finally, cells are plated up to a final concentration of 20.000 cells cm^{-2}, incubated at 37 °C and 5% CO_2 in cellular growth medium (DMEM with 10% FBS, 100 µg ml^{-1} penicillin and 100 µg ml^{-1} streptomycin). From now on, cells start to replicate up to cover all the glass substrate: this process happens in few days or up to a week depending on the initial concentration of cells. If the latter is low, i.e. 10%, cells can be found as single elements even after 24h. Initial concentrations of 50% and more give an almost complete coverage of the substrate after the same time. CP – NPs are loaded into the cells to give an optical density of 0.2. An amount of 50 µL of CP – NPs has been diluted in 1 mL of complete growth medium. After 24 hours' growth, cells are ready for experiments. Cells are cultured in multi well plates, thus twelve glass substrates are prepared. Six of them are endowed with the nanoparticles, the others are growth in common medium. For each substrate, two ROIs are selected. One is illuminated, the other is not. It acts as internal control, since it provides a direct comparison between illuminated and non – illuminated cells on the same glass substrate. The illumination duration is set to 2 minutes, with the cell in a bath of KRH. Then, KRH is washed out and the probe is administered to the cell, as described in *Methods – Molecular probes for Reactive Oxygen Species*. Imaging is performed by exciting the probe with the cyan LED (λ_{em} = 490 nm). The emission of the specimen passes through with FITC filter, that cuts out the emission of the nanoparticles. Therefore, the fluorescence signal can be associated only to the probe.

II.VII Hydra Vulgaris

Animal testing is mandatory to check whether our model works also in models more complicated than a single cell. To purchase this goal, we choose *Hydra Vulgaris* as living model. It is a small animal at the base of evolution. It's millimetric body is made of three parts: a disk-like foot, used for gripping the ground figure II.18), a long

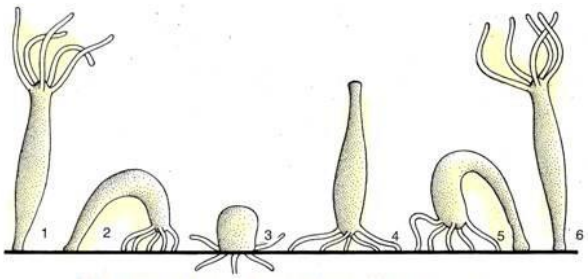

Figure II.18 Hydra vulgaris. Hydra is able to move following the steps in the figure.

body made of two epithelial layers and finally a set of six or seven tentacles. *Hydra Vulgaris* represent a very good compromise for animal testing for its lack of neurotransmitters. Therefore, there are no ethical involvements. They are able to regenerate whereas cut of parts occurred. Beyond those features, they present also a very fast reproduction. They are suitable also for light induced stimulation experiments, since their double epithelial layer is transparent. All those features, summed up with the high experimental throughput make those animals perfect candidates for *in vivo* assessment. They are cultured in a specific solution (Hydra solution, see Appendix C for composition) and fed three times a week. Their food is shrimp larvae (eggs of *Arthemia Nauplii*). CP – NPs have been administered to *Hydra* Vulgaris, whose bio-distribution and internalization has been investigated [15]. Internalization has been studied with the aim of inorganic fluorescent nanocrystals of different shape, ending with internalization by macropynocytosis and consequent accumulation in cytoplasmic vacuoles. For CP – NPs, studies of fluorescence microscopy provide macropinocytosis as internalization path. The same analysis gives the bio-distribution: figure II.19 shows bright field images on the left side and fluorescence images on the right side of the same region. The images on the top show the head of the animal with some tentacles, while the bottom ones are a focus on a tentacle tip. After few hours of incubation, nanoparticles are clearly in the ectodermal cells, appearing as fluorescent spots (excitation wavelength 470 nm). The tissue presents a huge number of cells with respect to the ones cultured on glass substrates. Therefore, higher CP – NPs concentrations are employed, 0.2, 0.4 and 0.6. The imaging

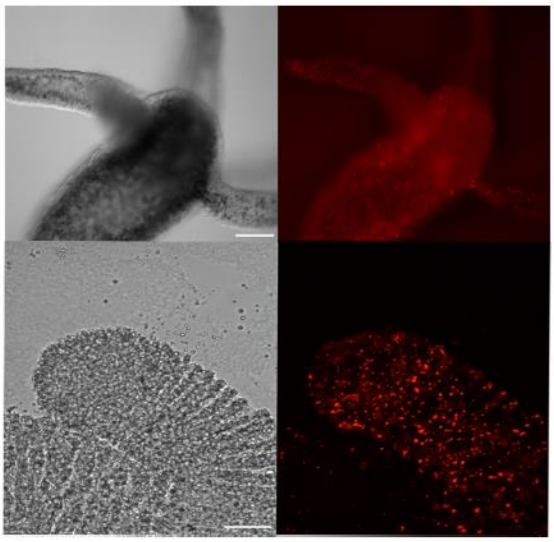

Figure II.19 Microscope image of Hydra Vulgaris. (Left) Bright field images of the head (top) and tentacle (bottom) of hydra. Fluorescence images (left) refer to bright field ones. The nanoparticles are clearly visible as red points.

technique is the one described before, thus the chosen spot size is 0.92 mm^2. Therefore, the whole hydra is too big to be imaged. Moreover, *hydrae* are able to move around in water environment just by releasing the grip of their foot. They also contract their body when feeling external stimulus, as mechanical and light ones. For these reasons, we decided to study imaging on slices of the animal, kept only from their body. To do so, the foot and the tentacles have been cut away, and the body has been

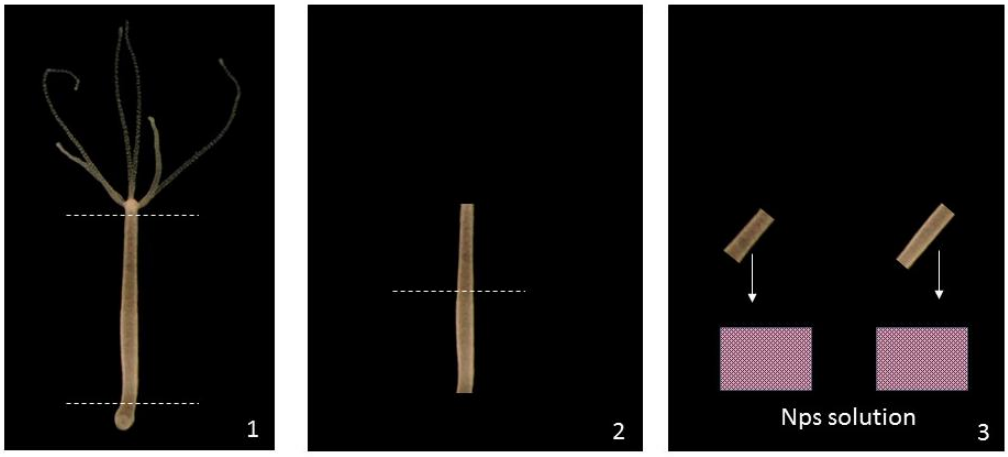

Figure II.20 Hydra sectioning for experiments. The panels describe the sectioning of the hydra. First, feet and tentacles are cut (1). Then, the remaining part of the body is cut in two more parts (2). Finally, each part is put in a solution of nanoparticles (3).

cut into two more little slices (figure II.20). *Hydrae* are first kept in a bath of nanoparticles for 24 hours. Then they are cut as shown in figure, each slice being put in a refilling solution of nanoparticles for 24 hours more. This because injuries provoke a local increase of ROS production, since they stimulate the cicatrisation. Thus, if we measure ROS concentration immediately after the healing, they are most probably

related to biological activities instead of nanoparticles' one. Conditions for the experiment are illuminated and not illuminated animals, each of them including animals treated with P3HT nanoparticles, polystyrene nanoparticles and wild type. Sets of five *hydrae* per condition are taken for the experiments.

Imaging cannot be performed with the 20x zoom, because *hydrae*'s pieces occupy the whole spot. This prevents to take the background, obtaining a not precise measure of fluorescence. Thus, images are taken with 4x zoom. One ROI includes the whole *hydra*'s piece, another the background. Thus, background is subtracted to the fluorescence coming from the *hydra*. Then, images are analysed with ImageJ software, following the same method of cell's imaging.

III. Experimental results and discussion

This section is dedicated to the description of the experiments and to the presentation of the results. First, an electrochemical characterization of the nanoparticles is provided. Second, ROS fluorescence imaging results are reported for the *in vitro* model. Ca^{2+} imaging results are presented and related to ROS ones. Finally, *in vivo* ROS measurements are reported.

III.I Superoxide electrochemical measurements

In order to check whether nanoparticles are producing O_2^-, measures with specifically functionalized electrodes are carried out. A modified gold electrode, functionalized as described in *Methods – Electrochemical measurement*, is used as working electrode. The reaction taking place are the following [28]:

$$cytC(III) + O_2^- \rightarrow cytC(II) + O_2 \quad (at\ electrode - electrolyte\ interface) \quad (2)$$

$$cytC(II) \rightarrow cytC(III) + e^- \quad (at\ electrode) \quad (3)$$

Therefore, taking the electrode at the oxidation potential of the cytochrome C, the second reaction is superimposed, leaving cytC(III) on the surface to react with superoxide. The second reaction is the one measured by the electrode, therefore we record a cathodic current (see appendix B). Cytochrome C is a haemoprotein: it consists of Fe^{2+} ion encapsulated in a macrocycle organic compound, a porphyrin. Figure III.1 shows the haem group (haem C) of the cytochrome.

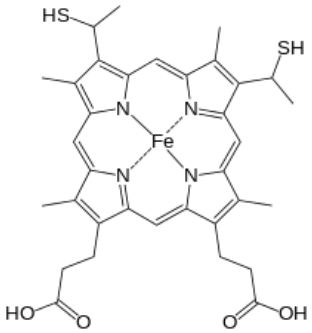

Figure III.1 Haem group of cytochrome C. The presence of Fe makes this compound able both to oxidize and reduce.

Figure III.2 reports on the chronoamperometries at cytochrome C oxidation potential, where the yellow box is related to photoexcitation time.

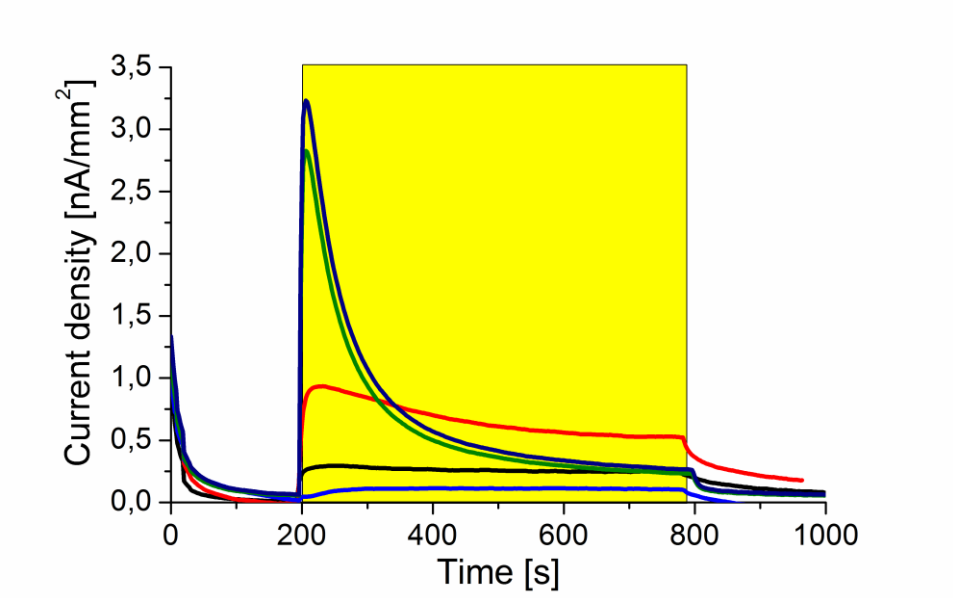

Figure III.2 Chronoamperometry at cytochrome C oxidation potential. This figure reports on the photocurrent generated by the compounds. The yellow box is related to the illumination interval. **Dark blue**: Au/NAC/CytC in PB solution. **Green**: Au + cytC solution. **Red**: Au/NAC + P4HT – NPs solution. **Black**: Au/NAC/CytC + P3HT – NPs solution. **Blue**: Au + NPs solution.

The positive current is associated to an electron flow from the electrode towards the electrolytic solution (cathodic current), that is the one described by reactions (2) and (3). Therefore, the curves associated with the P3HT – NPs solution (black, red, blue) denote their generation of electrons. Looking at the control (Au + NPs solution, blue), the activity of the nanoparticles is extrapolated, reported in detail in figure III.3.

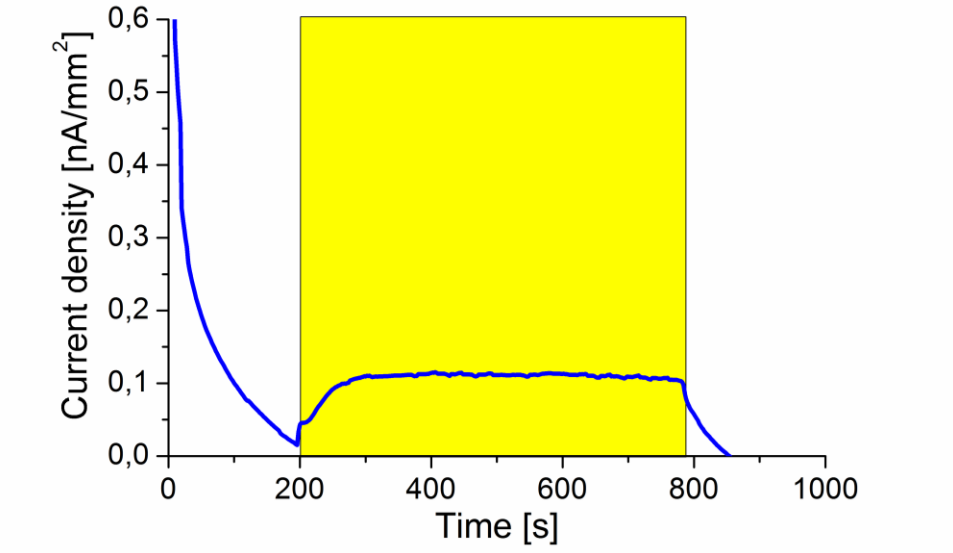

Figure III.3 Chronoamperometry at cytochrome C oxidation potential of P3HT - NPs vs Au electrode. The activity of the illuminated nanoparticles is reported. The yellow box is related to the illumination time.

They generate a self – sustaining current upon illumination. Cytochrome C solution and immobilized cytochrome C (olive and dark blue, respectively) present high light response, but a different dynamic with respect to the polymer's one. Functionalized electrodes (Au/NAC + NPs solution, red, Au/NAC/cytC + NPs solution, black) present a higher current response when nanoparticles are photoexcited. Moreover, Au/NAC electrode has a higher current response with respect to Au/NAC/cytC one. NAC is commonly used as radical scavenger [23], therefore it is sensitive to many radical species produced by the photoexcited nanoparticles. Cytochrome C is sensitive to O_2^-, thus the photocurrent is associated only to this radical.

Electron transfer can promote different oxygen reductions. Figure III.4 reports on the one electron reductions of oxygen whose redox potential is in the proximity of HOMO and LUMO levels of the polymer. The left side reports on the energy, while the right side shows the chemical reactions related to the oxygen reductions. Upon photoexcitation and subsequent relaxation, the polymer exhibits one electron at the

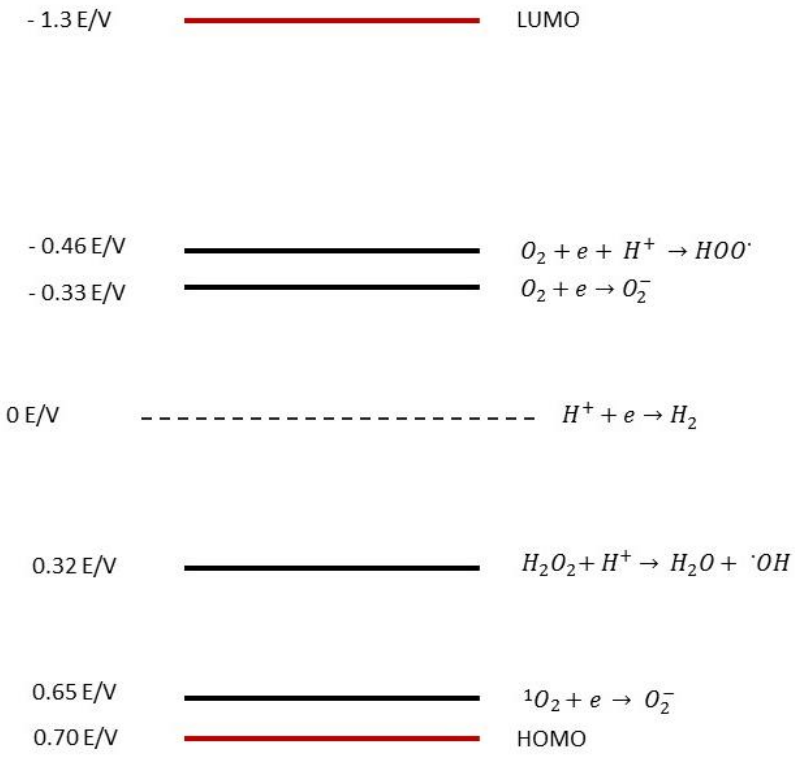

Figure III.4 Redox potentials of the possible reactions vs P3HT levels. On the left side there are the redox potentials of the reactions, while the right side reports on the related reactions.

LUMO level. Figure III.4 shows that there are at least two different reactions that can take place upon electron transfer, that is the generation of the superoxide and perhydroxyl radical. The reduction O_2/O_2^- agrees with the catalytic effect of polythiophene films in water suspension [12] and is the radical species detected by cytochrome C. The reduction $O_2,H^+/HOO\cdot$ is favoured whether nanoparticles are forming the photodoped complex $P3HT^+:O_2^-$ [14]. The intercalation of negative charges in the polymer surface leaves positive charges (H^+) in the solution, therefore the reduction $O_2,H^+/HOO\cdot$ happens.

Measures of immobilized cytochrome C photocurrent in phosphate buffer (dark blue) present a higher peak when the compound is photoexcited with respect to the same electrode in P3HT – NPs solution. This is ascribed to the **absorption of the P3HT – NPs**. To verify this hypothesis, we use the Lambert – Beer law

$$I(x) = I_0 e^{-\varepsilon x} \tag{4}$$

being I_0 the incident intensity, ε the absorption coefficient and x the distance at which the attenuation is calculated.

Figure III.5 presents the absorption spectrum of the P3HT – NPs solution used for the measurements, compared with the one of the cytochrome solution. At the selected

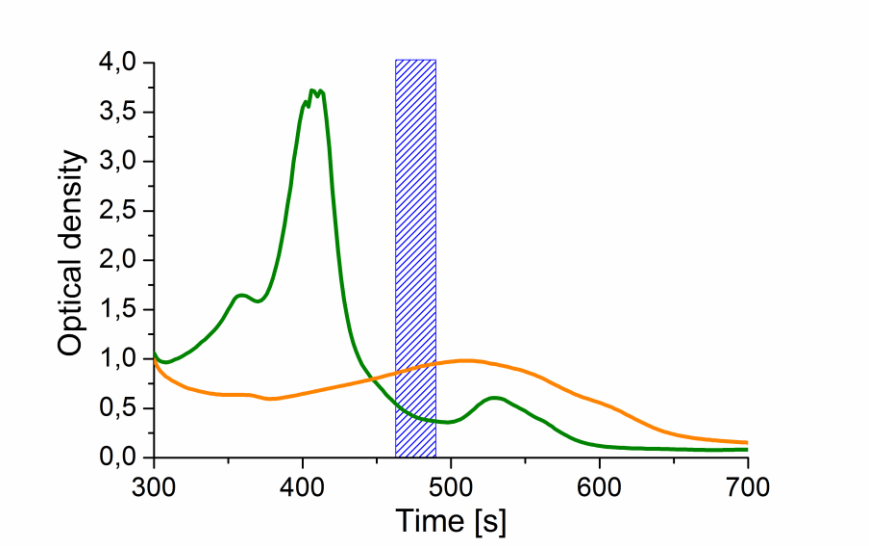

Figure III.5 Absorbance of P3HT - NPs and cytochrome C. The absorbance of P3HT – NPs in phosphate buffer and cytochrome C (in phosphate buffer) are reported. The blue box corresponds to the excitation wavelength (470 nm), being the thickness equal to the full width at half maximum of the employed LED. At that wavelength, the absorbance of the Cytochrome C is lower than the one of the nanoparticles.

wavelength (470 nm) the optical density is 0.88. This value is related to an optical path of 4 mm, therefore the extinction coefficient of P3HT – NPs solution is

$$\varepsilon_\lambda = {}^{OD}/_{L} = {}^{0.88}/_{4\ mm} = 220\ m^{-1} \quad (5)$$

Before reaching the electrode, photons cross a region of $\bar{x}$ = 5 mm of P3HT – NPs: being the incoming intensity I_0 = 2,7 mW mm^{-2}, the intensity that reaches the electrode (and so the cytochrome layer) is

$$I\ (\bar{x}) = I_0 e^{-\varepsilon \bar{x}} = 0{,}898\ {}^{mW}/_{mm^2} \quad (6)$$

Thus, the light impinging on the electrode is 30% of the incoming one. Comparing the current peaks of cytochrome in P3HT – NPs and phosphate buffer solutions, we get the same decrease for the signal of the immobilized cytochrome C. Thus, the hypothesis of ascribing the difference between these signals to the absorption of the P3HT – NPs is assessed. There is also a small difference between the immobilized cytochrome C and the solution: the former presents a higher peak value with respect to the latter. This is attributed to the proximity of the immobilized cytochrome C with respect to the electrode, that does not hold for the solution.

The activity of cytochrome C is under study, for its ability of acting as a photodiode [29] or as biosensor [19]. Its haem unit is like a semiconductor that undergoes light absorption, exciton formation and charge separation [30] [29]. The surrounding groups (porphyrin) are intrinsically insulators, thus they govern the transport of photogenerated charges from the haem unit towards the NAC sites. The dynamic of the photocurrent related to cytochrome C films has been intensively studied [29]. The decay has been quantified by interpolating the obtained curves with the exponential law $I = I_0 + Ae^{-t/\tau}$, being I_0 the dark current, A a constant parameter, t the time and τ the decay constant. Interpolating the obtained curve with the exponential law, we end up with a decay time τ = 200 s, in agreement with the reported one (τ = 162 ms [29]).

Integrating in time the current density dynamics, we obtain the number of collected charges. Defining t_1 = 200 s and t_2 = 600 s as the integration range, I_{ph} as the photocurrent, the charge density is

$$Q = \int_{t_1}^{t_2} I_{ph} dt\ = 3{,}94495 \cdot 10^{11}\ {}^{charges}/_{mm^2} \quad (7)$$

in the hypothesis of a Faradaic yield equal to 1, calculated for the Au electrode + NPs solution. **Charge generation** can be estimated considering the variation of population induced by photoexcitation:

$$\frac{\partial N}{\partial t} = G - R \tag{8}$$

Equation (8) ascribes the temporal variation of population to two terms, G and R, the former standing for generation and the latter for recombination. The stationary population density is given by

$$\mathcal{N} = G\tau = \varphi \frac{IA}{h\upsilon}\tau \frac{1}{V} \tag{9}$$

The excitons able to escape are those generated in the external shell of the nanoparticle whose thickness is equal to the exciton diffusion length, that is 20 nm. Thus, $V = {}^{4}/_{3}\,\pi(r^2 - (r - 20\,nm)^2)$. The excitation beam does not illuminate the whole area of the nanoparticle. In the hypothesis that half of the area is illuminated, we obtain $A = 2\pi r^2$. The power density is I = 2,7 mW/mm^2, the photon energy is hν = 2,23 eV. Considering a quantum yield φ = 10^{-5} we get a stationary population density per nanoparticle of $\mathcal{N} \cong 10^{15}\ mm^{-3}$, having considered a lifetime of 1 s [11]. The difference with those measured by electrochemistry is justified considering a Faradaic yield lower than 1.

III.II ROS imaging *in vitro*

P3HT – NPs production of superoxide has been demonstrated with electrochemical methods. Therefore, is reasonable to think at a similar behaviour in the cellular environment. As described in methods, the cellular model used for this experiments are HEK cells. They are plated on glass substrate with the P3HT – NPs in the extracellular solution from the very first moment. ROS are measured with three different fluorescent probes, with a peculiar specificity.

Figure III.6 presents a simplified scheme of the experimental setup for ROS

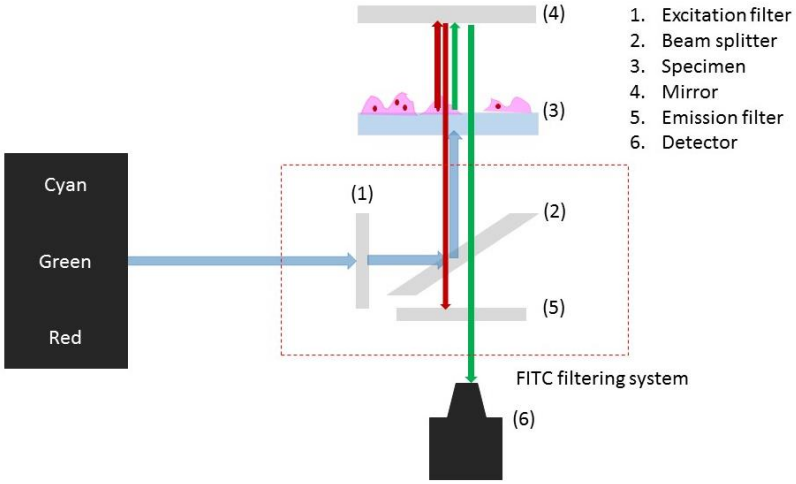

Figure III.6 ROS imaging setup for in vitro samples. The setup employs a FITC filter to cut nanoparticle fluorescence. Thus, only the signal related to the probe reaches the detector.

imaging. Light crosses the glass substrate before reaching the cells that have internalized the nanoparticles, resulting in photoexcitation of the polymer in cellular environment. Since cell's internal environment is constituted by a liquid substance (internal matrix), we can treat it as an isotropic diffusing medium, so the generated ROS diffuse in the whole cell. There are two issues to be pointed out. First, since ROS are usually produced by cells, the problem is to distinguish whether the presence of nanoparticles increases the ROS yield from the cell or nanoparticles are directly producing ROS. Second, we want to identify which ROS are produced. To check both these aspects, the measurement of the fluorescence of the illuminated samples is compared with different controls. Comparison between illuminated nanoparticles and illuminated cells allows to discriminate the effects of the photoexcited polymer and the effect of the light on cell physiology. The effects of the presence of the nanoparticles is studied within two controls: one with polystyrene nanoparticles (PS – NPs) of the same dimension, being not photosensitive, the other with non – treated cells. All are distinguished between illuminated and non – illuminated. The probes are H_2DCF – DA, APF and HPF, whose selectivity is reported in table III.1.

Table III.1 Probe selectivity.

Probe	Sensitive to (ordered by decreasing sensitivity)
H_2DCFDA	·OH, $ONOO^-$, ROO·, H_2O_2
APF	^-OCl, ·OH, $ONOO^-$
HPF	·OH, $ONOO^-$, ^-OCl

The first probe is H_2DCF – DA, that exhibits sensitivity to many types of ROS, as hydrogen peroxide and hydroxyl radical. Figure III.7 reports on the results. Illuminated nanoparticles present an increment of the 500% in ROS production with respect to illuminated control. Conversely, non – illuminated P3HT – NPs and control samples present the same ROS concentration. Therefore, the ROS concentration is modulated by photoexcited polymer.

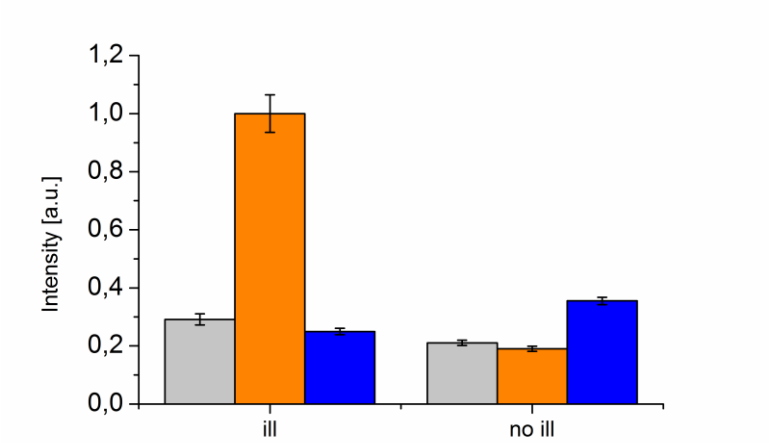

Figure III.7 H_2DCFDA fluorescence response in HEK cells. The bar diagrams are related to the intensity of the fluorescent probe in HEK cells. **Grey**: controls. **Orange**: P3HT – NPs. **Blue**: PS – NPs. The values are related to the mean over N = 100 cells, presented with the standard error of the mean. Illuminated samples are photoexcited for 2 minutes with green light, while non – illuminated samples are directly incubated with the probe.

Then, results for APF and HPF are reported, the former being sensitive to hydroxyl radical and hypochlorite radical, the latter being sensitive only to hydroxyl radical. Figure III.8 presents the results obtained for APF (a) and HPF (b). APF presents a

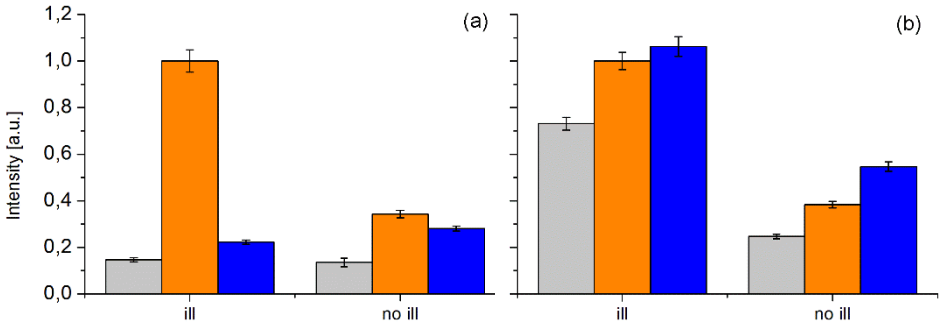

Figure III.8 APF (a) and HPF (b) fluorescence response in HEK cells. The bar diagrams are related to the intensity of the fluorescent probe in HEK cells. **Grey**: controls. **Orange**: P3HT – NPs. **Blue**: PS – NPs. The values are related to the mean over N = 100 cells, presented with the standard error of the mean. Illuminated samples are photoexcited for 2 minutes with green light, while non – illuminated samples are directly incubated with the probe.

fluorescence increment of 500% when nanoparticles are illuminated, with respect to illuminated control. Non – illuminated P3HT – NPs present a fluorescence increase of 200% with respect to non – illuminated control. Fluorescence related to polystyrene NPs is comparable to control levels. HPF shows an increment of 140% for illuminated

P3HT – NPs samples with respect to illuminated control. Even though, HPF presents a higher control level with respect to APF under illumination. Therefore, the effects of the photoexcited nanoparticles give a lower response in the case of HPF compared with APF and H_2DCF – DA. All present a high reactivity with the radical ·OH, therefore P3HT – NPs are producing this species when photoexcited. The fluorescence response of HPF shows an effect due to bare illumination, that is not polymer – mediated.

The previous experiments confirm the increase of ROS inside cells when P3HT – NPs are photoexcited. It is still unclear whether cells undergo oxidative stress or polymer interacts with the intracellular environment. In the latter, cell can also undergo thermal stress, therefore an estimation of the induced temperature variation is mandatory.

Thermal effect has been demonstrated to be induced in HEK cells by blend of polythiophene films [13]. HEK cells have not thermal gated channels on their own, but by DNA transfection is possible to activate them. Therefore, transfected HEK cells present specific channels that are activated by temperature changes (TRPV1). An estimate of the temperature increase during photoexcitation of nanoparticles can be done, starting from Fourier law (10),

$$Q = -k\nabla \boldsymbol{T} \tag{10}$$

Referring to equation (10), Q is the heat flux, k is the thermal conductivity and **T** is the function describing the temperature changes in the whole space. Simplifying to a 1D problem, the gradient is just a spatial derivative. In our case, the heat flux is represented by the irradiation density power, I. Calculating the integral, we get:

$$Q = -k\frac{dT}{dx} \rightarrow \int_0^r Q dx = \int_{T_i}^{T_f} (-k dT) \tag{11}$$

$$Q = I = {}^{k(T_i - T_f)}/_{r} \tag{12}$$

Equation (11) shows the dependence of the heat energy with respect to the distance. It results to be an inverse dependence, therefore the higher the distance, the lower the effects of the heating. Once internalized, nanoparticles are embedded with the inner cellular environment, therefore local increases in temperature can activate membrane channels. The power density of our illumination is $I = 54.34\ {}^{mW}/_{mm^2}$, the radius of the nanoparticle is on average 200 nm. Thermal conductivity of intracellular solution is $0.6\, Wm^{-1}K^{-1}$. Considering the heat to be uniformly

generated in the whole nanoparticle, by Fourier equation we can calculate the temperature increase provoked by one nanoparticle at a distance equal to its radius for instance. Thus, introducing these numbers in equation (12) we get a generated thermal increase of $\Delta T = 18\, mK$. One nanoparticle induces a very small thermal variation. Thus, evaluation of the temperature increases of aggregates is mandatory. In the hypothesis of 100 nanoparticles whose aggregate can still be approximated with a sphere, we end up with a radius of 20 µm. It generates a temperature increase of $0{,}18\, K$. It is a quite change in temperature, therefore the analysis of temperature gated channels has been performed. Measures taken on transfected HEK cells are reported in figure III.9, showing the response of the membrane potential to light stimulus. This measure is performed with the patch clamp technique. It consists in

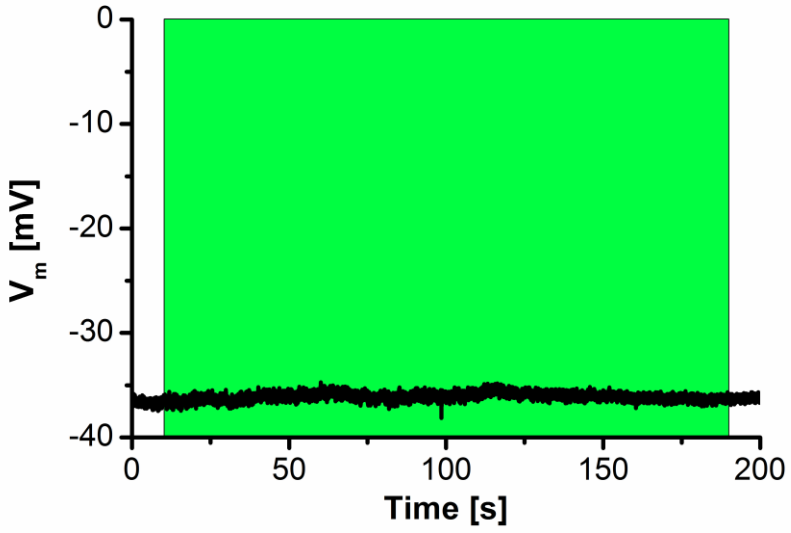

Figure III.9 Transfected HEK cells' light response. The membrane potential (Vm) is measured with respect to time. The green box is related to the illumination time interval. Figure shows one representative curve of a sample of N = 4.

putting a micropipette in contact with the membrane, across which the ions of the selected channel can pass. Another pipette is grounded, so the voltage drop across the cell membrane is measured. Thus, the technique allows to measure one cell at time, that's why the 40x zoom has been used for this experiment. Cells that are in contact with each other can communicate through ion channels, thus the membrane responses can be related to the intercommunications rather than stimulation. Changes in this potential drop are identified as a depolarization and a subsequent hyperpolarization, while no activation shows a constant potential also during the stimulus. Figure III.9 shows the response of the membrane potential to an illumination lasting 3 minutes, under a power density of 217.39 mW/mm^2. The increase in the power density reflects on the thermal increase, being 72 mK per nanoparticle. Light

induces no variations, therefore there are no activated temperature – gated ion channels. All these reasons confirm the hypothesis that P3HT – NPs are not inducing thermal stress to the cells.

III.III Ca^{2+} and ROS

As mentioned in the introduction, Ca^{2+} is a key- messenger with many different functions in several cellular physiological activities, including, just to cite some, cell growth and proliferation, regulation of enzyme activity, activity of ion pumps, intra- and inter-cellular signalling pathways, cytoskeleton modulation, neuronal synapsis. Thus, the study of calcium dynamics in presence of specific stimuli (in our case, light and polymer nanoparticles) harvest huge interest in both excitable and non-excitable cells. Cells are plated on glass substrates in the culture medium. The three conditions are untreated cells, P3HT – NPs treated cells and PS – NPs treated cells. The nanoparticles are added during the plating. After 24 hours, Ca^{2+} is measured upon light stimulus with a fluorescent Ca^{2+} indicator.

Figure III.10 presents the dynamics of Ca^{2+} in HEK cells for different conditions. Untreated cells (control) dynamics are compared with those of cells treated with P3HT and PS - NPs. The intensity is related to the probe response to Ca^{2+} concentration in the cells, therefore is directly connected with the Ca^{2+} dynamics. Each panel shows three representative curves (related to three cells), even if each condition has been measured with N = 100 cells. Results (figure III.1) are distinguished between the two different extracellular solutions, KRH and KRH Ca^{2+} free. Being Ca^{2+} both internalized from the extracellular solution and released by internal compartment, comparison between KRH and KRH Ca^{2+} free allow to distinguish the source of Ca^{2+} dynamic. As described in chapter II.II, is not possible to excite the nanoparticles and record the probe response at the same time. Therefore, we decided to employ two different powers, P_{LOW} = 34,78 mW/mm^2 and P_{HIGH} = 247,82 mW/mm^2, assuming the first as control. This because the lower power density is assumed to be exciting the nanoparticles less than the higher power density. Thus, the effects of the nanoparticles become preponderant only in the second case.

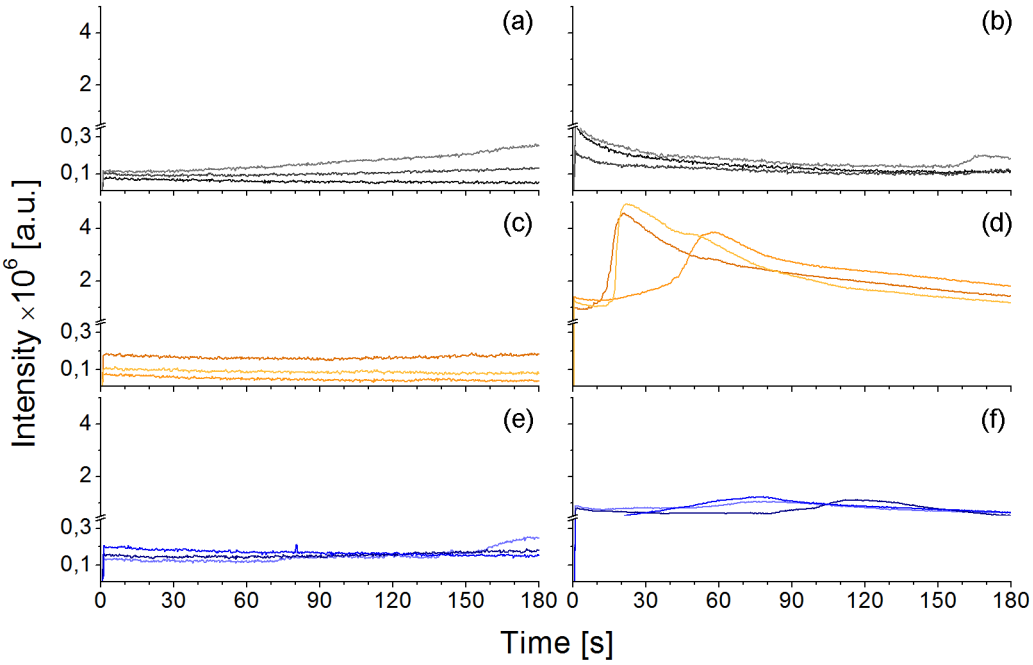

Figure III.10 Ca^{2+} dynamics in KRH Ca^{2+} free solution. Each panel shows Ca^{2+} dynamics for three representative cells. Panels (a) and (b) are showing untreated samples, at P_{LOW} and P_{HIGH} respectively. Panels (c) and (d) are showing P3HT – NPs treated samples, at P_{LOW} and P_{HIGH} respectively. Panels (e) and (f) are showing PS – NPs, at P_{LOW} and P_{HIGH} respectively.

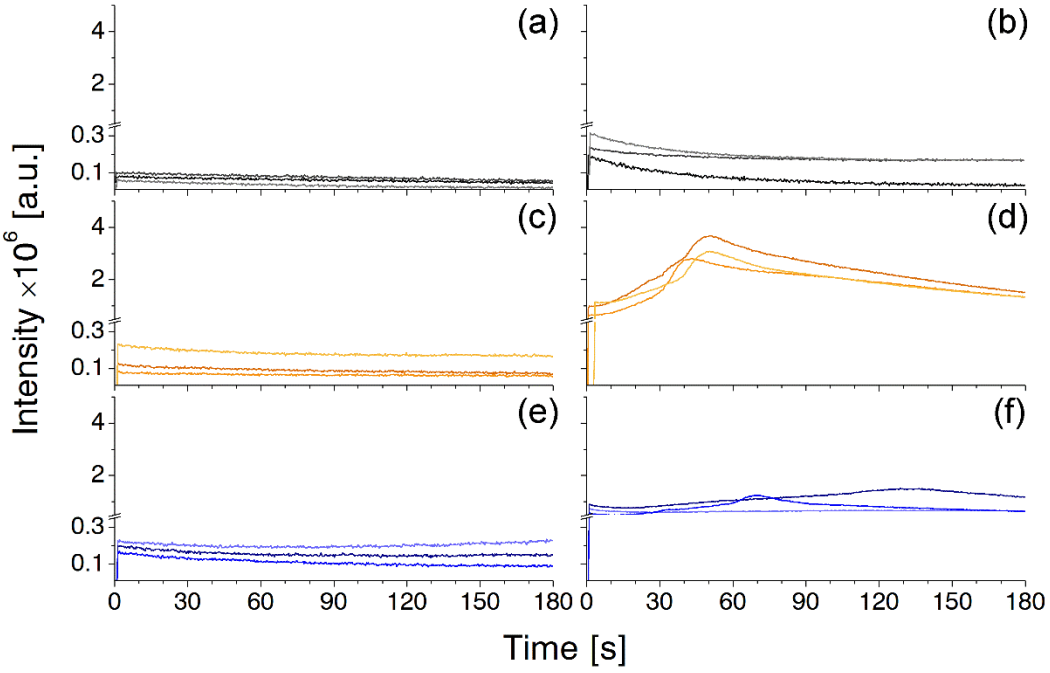

Figure III.11 Ca^{2+} dynamics in KRH solution. Each panel shows Ca^{2+} dynamics for three representative cells. Panels (a) and (b) are showing untreated samples, at P_{LOW} and P_{HIGH} respectively. Panels (c) and (d) are showing P3HT – NPs treated samples, at P_{LOW} and P_{HIGH} respectively. Panels (e) and (f) are showing PS – NPs, at P_{LOW} and P_{HIGH} respectively.

Measurements at P_{LOW} present no Ca^{2+} dynamic in all the conditions. Conversely, measurements at P_{HIGH} present a rising and falling profile, attributed to a changing concentration of the intracellular calcium levels. The photoexcited polymer presents a higher Ca^{2+} dynamic with respect to controls, both in the cases of KRH and KRH Ca^{2+} free. In absence of external Ca^{2+}, the difference between control and P3HT – NPs is higher with respect to the case of complete extracellular solution. To better appreciate this difference, figure III.12 reports on the ranges (peak – basal level) for all the conditions. Photoexcited P3HT – NPs increase the response of intracellular Ca^{2+} levels,

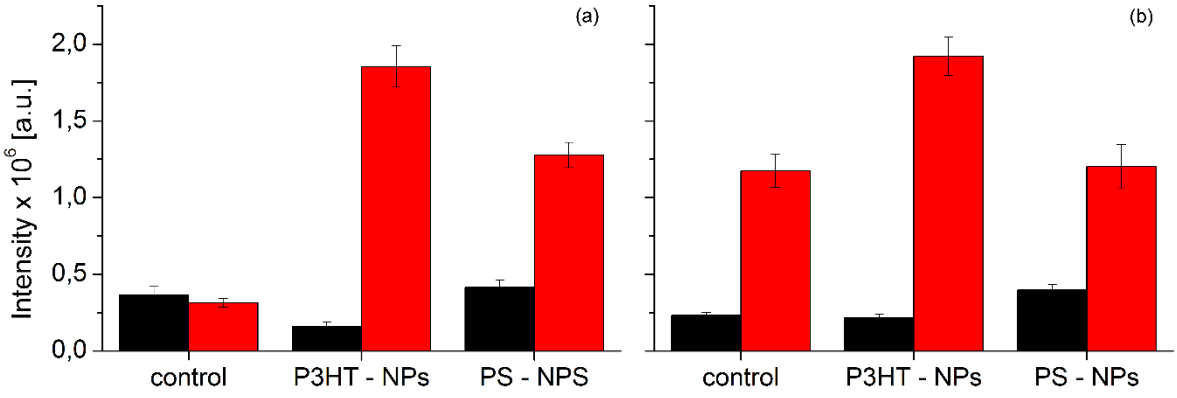

Figure III.12Peak analysis of Ca^{2+} dynamics. Bar diagrams represent the values of the range (peak – basal level) of the dynamics shown in figure III.10 and III.11. They are normalized with respect to the value of P3HT – NPs at PHIGH. The values in black are related to P_{LOW}, while the values in red are related to P_{HIGH}.

generating a higher concentration calcium wave with the respect to control. This increment is higher in the case of KRH Ca^{2+} free. Calcium fluxes can be both associated to internalization from external environment and release from inner compartments, as endoplasmic reticulum. Therefore, the result obtained in KRH Ca^{2+} free condition assesses that the polymer is acting on internal calcium changes. PS – NPs present a higher signal with respect to control, but the difference is lower with respect to P3HT – NPs. This effect is attributed to the high scattering contribution of polystyrene NPs.

It is well known that calcium dynamics regulate, among many other physiological functions, also the intracellular levels of ROS. Physiological ROS levels are key to maintain the correct homeostasis of the cell, to guarantee the respiration process and to modulate many other cellular activities. On the other hand, ROS over-production is also a well – known protection mechanism by which the cell reacts to the presence of external bodies or potentially toxic stimuli. We hypothesized that the observed increased dynamics of intracellular calcium concentration may be related to

the treatment of cells by polymer NPs and light, leading to enhanced ROS production. In order to validate this hypothesis, we carried out measurements with inhibition of ROS, that is NAC. Extracellular solution with NAC is used during the stimulus, both for KRH and KRH Ca^{2+} free. Results are presented in figure III.13 and III.14.

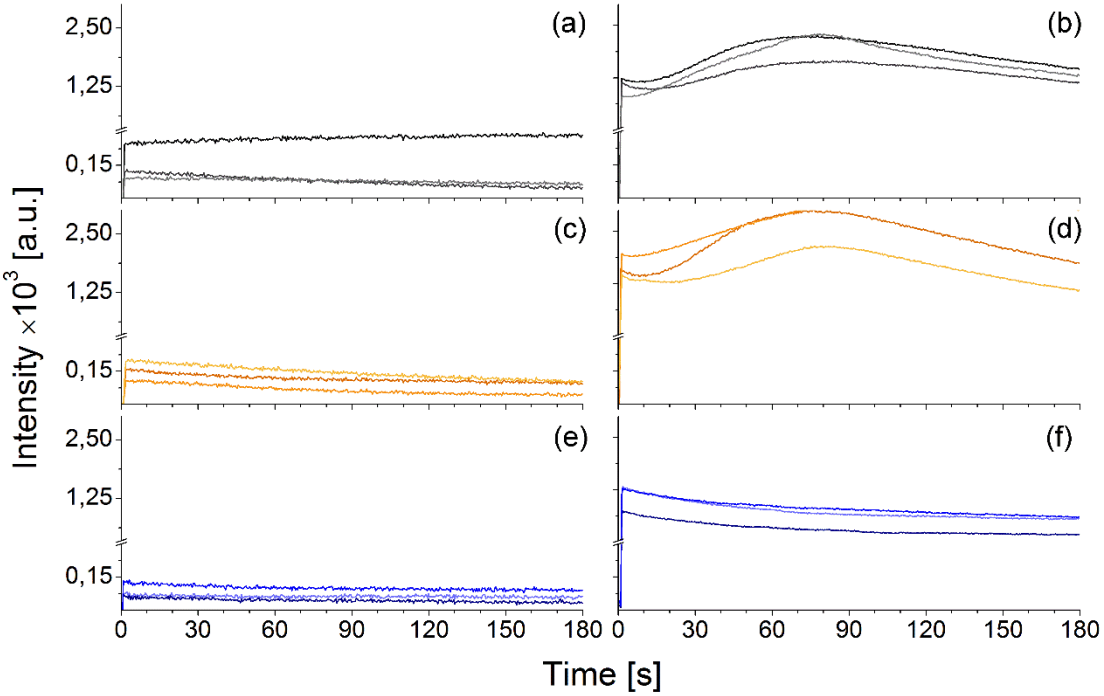

Figure III.13 Ca^{2+} dynamics in KRH Ca^{2+} free + NAC solution. Each panel shows Ca^{2+} dynamics for three representative cells. Panels (a) and (b) are showing untreated samples, at P_{LOW} and P_{HIGH} respectively. Panels (c) and (d) are showing P3HT – NPs treated samples, at P_{LOW} and P_{HIGH} respectively. Panels (e) and (f) are showing PS – NPs, at P_{LOW} and P_{HIGH} respectively.

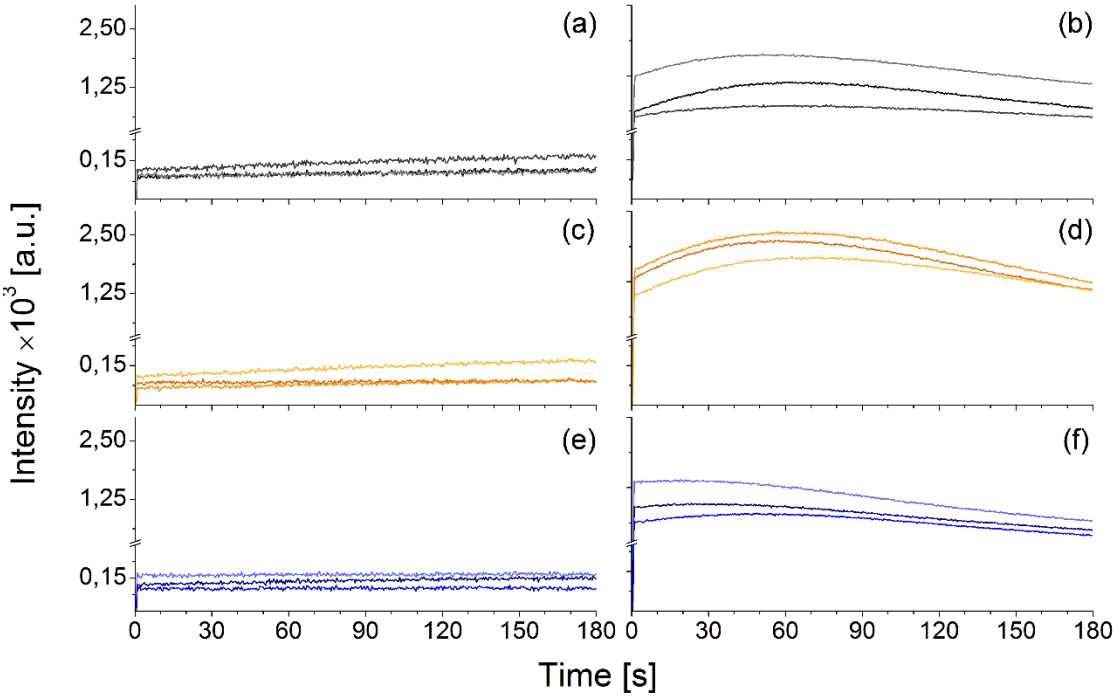

Figure III.14 Ca^{2+} dynamics in KRH + NAC solution. Each panel shows Ca^{2+} dynamics for three representative cells. Panels (a) and (b) are showing untreated samples, at P_{LOW} and P_{HIGH} respectively. Panels (c) and (d) are showing P3HT – NPs treated samples, at P_{LOW} and P_{HIGH} respectively. Panels (e) and (f) are showing PS – NPs, at P_{LOW} and P_{HIGH} respectively.

In all the cases, the signals are not showing Ca^{2+} dynamics. Comparing the achieved results with the ones without the ROS inhibition, the absence of a calcium dynamic is straightforward. Therefore, the inhibition of ROS inhibits the calcium dynamics, too.

Cross-talk between Ca2+ and ROS signalling systems occurs at multiple levels (figure III.4) in different subcellular compartments (e.g., the plasma membrane, the cytosol and mitochondria), and involves a constellation of molecular players [25]. Excitable cells are dramatically affected by Ca^{2+} concentration changes, being their

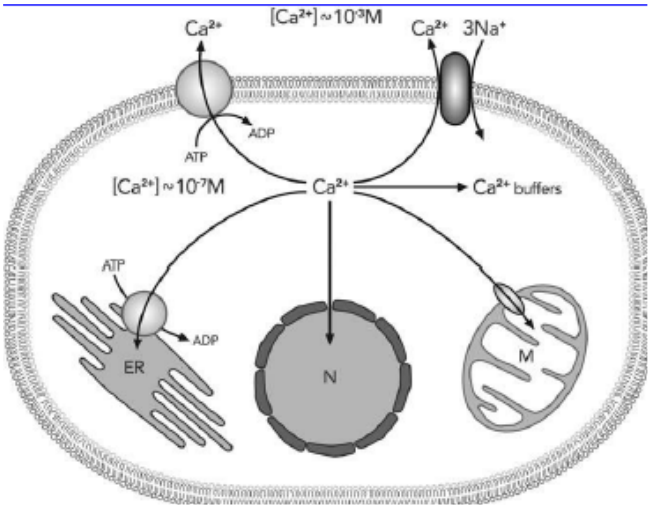

Figure III.15 Ca2+ - ROS cross talk. The inner compartmets as mitochondria and endoplasmic reticulum possess Ca^{2+} pumps in the memrane

membrane endowed with Ca^{2+} channels. Besides non – excitable cells do not present the same channels, the Ca^{2+} regulation affects many physiological activities. Ca^{2+} is contained in endoplasmic reticulum (ER), in the nucleus and in the mitochondria. All of them are encapsulated in a membrane that provides receptors able to regulate calcium homeostasis. They are ryanodine receptor (RyR) for excitable cells and inositol 1,4,5 – trisphosphate receptor (IP_3R) for non - excitable ones. Ca^{2+}/ROS interaction in the nucleus can affect gene expression [26], this effect being still under studies. Mitochondrial variations in Ca^{2+}/ROS concentrations are mostly related to cell apoptosis [18]. HEK 293 cells treated with P3HT – NPs show positive results to MTT assay, therefore they do not exhibit apoptosis. ER Ca^{2+} release via IP_3R is initiated by binding of the signalling molecule IP_3. Sensitization of IP_3R to IP_3 through modulation of thiols has been observed in response to ROS derived from xanthine oxidase [27]. The oxidation of IP_3R by ROS results in depletion of mitochondrial Ca^{2+} towards the cytosol [25]. Data previously reported assess that P3HT – NPs affect internal calcium concentrations without inducing apoptosis, therefore they are acting on ER calcium homeostasis. The release in the cytosol is the measured increase in concentration, since the probe is diffused in the cytosol, too.

Ca^{2+} and ROS interaction mediated by P3HT – NPs results to be a parallel interplay that we proved by inhibiting ROS in the cytosol. Therefore, photoexcited P3HT – NPs are able to generate ROS in cellular environment.

III.IV ROS imaging in vivo

Hydra vulgaris is an invertebrate animal. It is a good model for *in vivo* experiments, therefore we used it to check whether the results achieved for the *in vitro* model are the same of the *in vivo* ones. *Hydra* responds to perturbations mainly by contractions and movements, therefore maintaining the animal in the same position is not an easy task. As described in methods (chapter II.VII), tentacles and foot are cut away and the body is divided into two more parts. The same probes (H_2DCF – DA, APF, HPF) of the cells are used to focalize which ROS are involved in the processes. Moreover, since we are handling tissues, we employ three different optical densities, OD = 0.2, OD = 0.4, OD = 0.6. Figure III.16 shows the response of internalized DCF. It shows a higher production of ROS by P3HT – NPs with respect to polystyrene ones and wild type. Therefore, the data confirm the same behaviour of the cells for this kind of probe. The concentration dependence does not respect the expected behaviour: we expect a higher ROS production with increasing P3HT – NPs optical density. Results

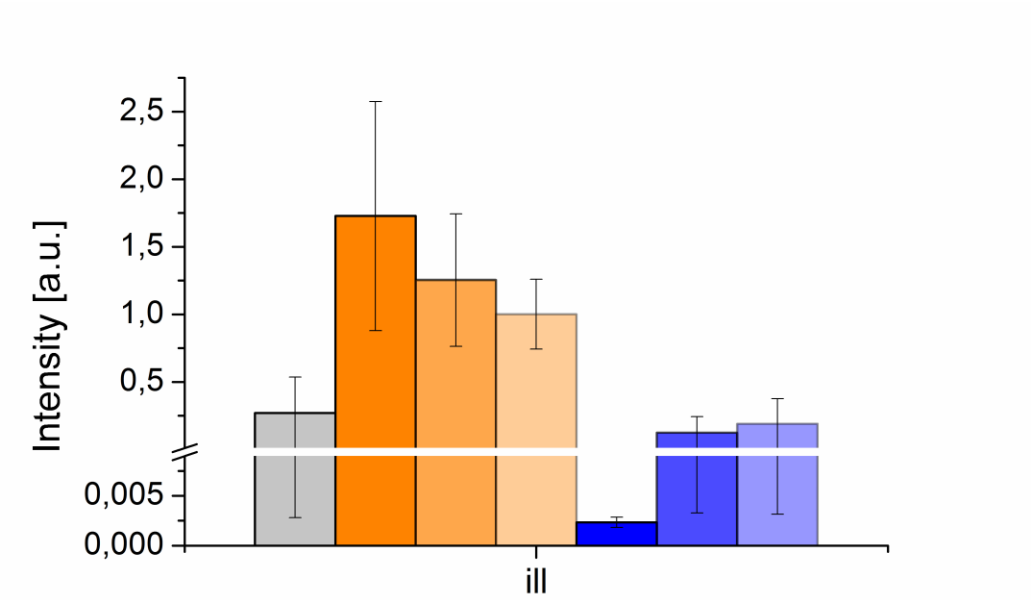

Figure III.16 H_2DCFDA fluorescence response in Hydra Vulgaris. The bar diagrams are related to the fluorescence value of the probe. **Grey:** control. **Dark orange**: P3HT – NPs with OD = 0.2 treated animals. **Orange:** P3HT – NPs with OD = 0.4 treated animals. **Light orange**: P3HT – NPs with OD = 0.6 treated animals. **Dark blue**: PS – NPs with OD = 0.2 treated animals. **Blue**: PS – NPs with OD = 0.4 treated animals. **Light blue**: PS – NPs with OD = 0.6 treated animals. Bars are related to fluorescence values averaged over N = 5 animals. Measures are reported with the standard error. P3HT – NPs show higher fluorescence response with respect to PS – NPs and to control. They also exhibit a decreasing behaviour with respect to the increasing optical density.

show, instead, a reduction of produced ROS by P3HT – NPs. This can be ascribed to a re – absorption effect: P3HT absorption spectrum partially overlaps the emission of the probe. Therefore, the increase in the optical density is the effect of the nanoparticles that are absorbing the photons emitted by the DCF. Estimation of the re – absorption of the nanoparticles can be done by evaluating the cross correlation between the two spectra. Let ϕ_{DCF} be the emission spectrum of the probe and ϕ_{P3HT} to be the absorption spectrum of the P3HT – NPs. The cross correlation is given by equation (13),

$$R(\lambda) = \int_{\lambda_1}^{\lambda_2} \phi_{DCF}(\xi)\phi_{P3HT}(\lambda + \xi)\, d\xi \qquad (13)$$

It gives back the number of photons of the emission spectrum that is re – absorbed by the P3HT – NPs. In our case, it is not possible to achieve the exact spectrum of the probe for its light induced auto – oxidation, that gives different results even for samples kept in the same conditions. Therefore, we rely on the spectrum of the datasheet, that is normalized. Thus, the cross correlation gives only the overlap fraction of the two spectra. The cross correlation has been calculated using Matlab. Figure III.17 (b) reports on the reabsorption calculated as the overlap between

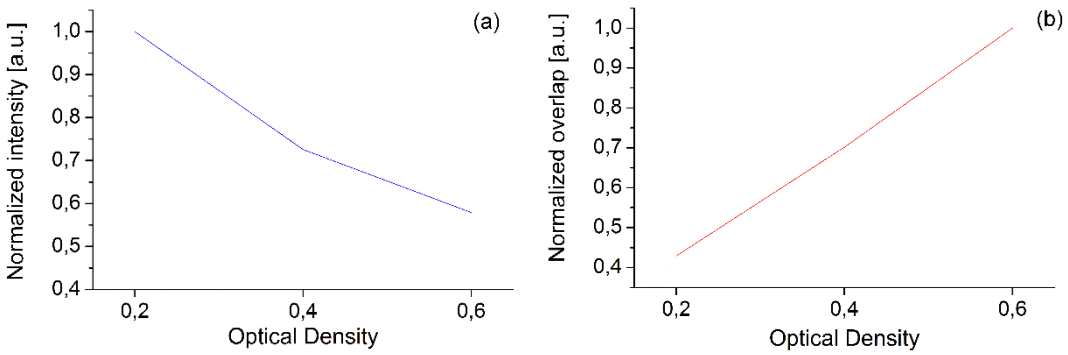

Figure III.17 Probe emission (a) vs calculated re - absorption (b). Panel (a) shows the probe emission vs optical density, having considered the maximum values of the bar diagram of figure III.13. Panel (b) reports on the re – absorption of the nanoparticles, calculated as the overlap between the P3HT – NPs absorption and probe emission spectra. Both present a linear trend, thus the hypothesis of the re – absorption of the nanoparticles to explain the decrease in fluorescence with the optical density is confirmed.

absorption and emission of nanoparticles and probe, respectively, while figure III.17 (a) reports on the emission of DCF from *hydrae*'s body. Calculated re – absorption shows a linear behaviour. Conversely, P3HT – NPs' emission is affected by second order effects. Reasonably, the same holds for the re – absorption of nanoparticles. The difference in optical density reflects a difference in concentration. At higher concentration, there is a higher number of nanoparticles in contact with the probe,

therefore the re – absorption effect is more probable, being P3HT – NPs and probe's molecules closer. Moreover, we have to consider the scattering effect of *hydra*'s tissue, that is not included in the re – absorption model. Since these processes are not included in the theoretical calculation of the re – absorption, the obtained linear behaviour is in reality superimposed by second order effects.

Figure III.18 shows the response of APF (a) and HPF (b), where the experiments are performed in the same conditions of the previous probe. APF incubated in P3HT – treated samples exhibit no fluorescence changes with respect to wild type. The

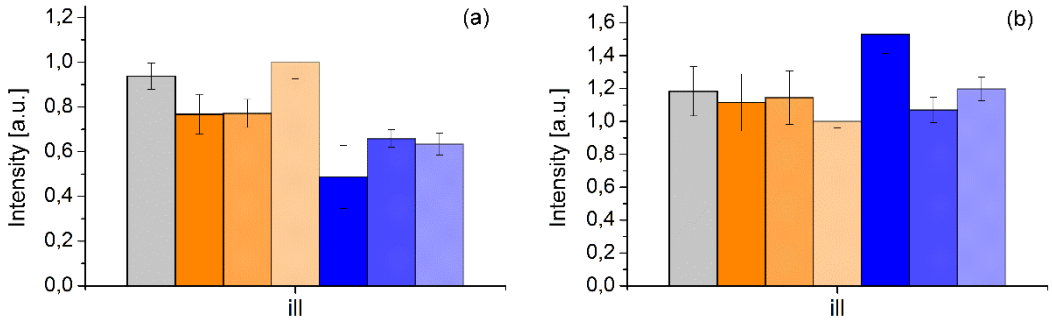

Figure III.18 APF (a) and HPF (b) fluorescence response in Hydra Vulgaris. The bar diagrams are related to the fluorescence value of the probe. **Grey:** control. **Dark orange**: P3HT – NPs with OD = 0.2 treated animals. **Orange:** P3HT – NPs with OD = 0.4 treated animals. **Light orange**: P3HT – NPs with OD = 0.6 treated animals. **Dark blue**: PS – NPs with OD = 0.2 treated animals. **Blue**: PS – NPs with OD = 0.4 treated animals. **Light blue**: PS – NPs with OD = 0.6 treated animals. Bars are related to fluorescence values averaged over N = 5 animals. Measures are reported with the standard error. There are no significant differences, thus the ROS to which APF and HPF are sensitive are not produced in the hydra.

fluorescence response of the polstyrene is lower with respect to both wild type and nanoparticles. The same holds for HPF. There results are in disagreement with the *in vitro* ones. *Hydrae* biology is different with respect to HEK cells. Moreover, APF and HPF are selective to hydroxyl and hypochlorite radicals. Therefore, a reasonable hypothesis for this behaviour stands in the fact that *hydrae'*s cells are not producing the ROS to which APF and HPF are selective. Moreover, the probes in *hydra* environment can experience quenching channels that are not present in the HEK cell system, for example scattering. The latter results to be predominant on the measure of generated ROS, therefore no appreciable changes are recorded between treated and wild type samples. The re – absorption effect is missed, even if the emission and absorption spectra are still overlapped. Also this effects can be attributed to the high scatter effect of the tissue.

Hydra has been hystorically studied for its regeneration properties. Genes responsbile for regeneration have been demonstrated to be redox sensitive [31]. ROS signalling regulates both autocrine and paracrine immune responses, activating genes

that start regeneration processes. The result we obtained with H_2DCF – DA declare a ROS production increase mediated by P3HT – NPs.

IV. Conclusions and perspectives

This work has the aim of identifying the photo-actuation mechanism of polymer nanoparticles in *in vitro* and *in vivo* biological models.

First, the simplified system of polymer NPs in a biological-like buffer solution has been considered. The occurrence of photo-electrochemical phenomena, namely the production of Reactive Oxygen Species (ROS) has been evidenced by properly designed electrochemical experiments. More specifically, P3HT – NPs in aqueous dispersion result to generate a photocurrent signal. A dedicated functionalization of the electrode allows to selectively measure the generation of the superoxide radical anion, as the most probable generated species for thermodynamic and kinetic reasons. Results show that the signal has a strong light dependence, being activated only upon visible light illumination, matching the NPs absorption spectrum.

Direct measurements of ROS generated within the cell cytosol are then carried out. Cell samples treated with NPs and visible light confirm the previous finding, evidencing the enhanced production of ROS species, with statistically relevant differences respect to control samples (untreated and/or in dark and/or treated with inert polystyrene NPs). Reduced states of the molecular oxygen are identified *in vitro.* This phenomenon can be safely attributed to the occurrence of electron transfer reactions at the polymer/cytosol interface. A similar analysis has been carried out also *in vivo*, within the invertebrate *hydra* animal model. Results show a partial agreement with the *in vitro* ones, evidencing an enhanced production of ROS species. In this case, however, different ROS species are evidenced, possibly due to the huge difference in the cellular structure of the two models and to the higher complexity level of the animal model.

Finally, the biological effect of the ROS over-production is investigated. ROS enhanced levels turn out to be not toxic, and do not lead to apoptotic phenomena, nor to sizable effects on single cells/animal physiological activity. Still, changes in the intracellular ROS concentration is expected to have important outcomes on Ca2+ channels dynamics. The interplay between ROS and Ca^{2+} flux is, actually, a hot topic in the literature, being responsible for many physiological effects like, among others, specific enzymatic activation and regulation. The specific study of P3HT – NPs effects on the Ca^{2+} dynamics of HEK cells has been thus carried out. Results report on changes of Ca^{2+} dynamics mediated by the photoexcited polymer. Even more interestingly, inhibition of ROS production leads to the suppression of any change in Ca^{2+} dynamics, thus

confirming the mutual crosstalk between the photoelectrochemical reactions driven by the illuminated NPs and the physiological response of the living system.

Overall, this work focuses the attention on the possibility of using polymer hybrid interfaces as photo-electrochemical actuators. P3HT – NPs offer the possibility of achieving the modulation of biochemical messengers as Ca^{2+} and ROS by an injectable tool, without the help of external power supply. There are many aspects which worth further and extensive investigation, such as intensity- and time-dependent systematic studies, being these effects strictly related to charge photo-generation, photo-electrochemical reactions efficiency, and in the end to a mutual inter-communication between electronic and ionic transport. Considering the material design, core – shell nanoparticles, composed of an electron-donor and an electron-acceptor component, may provide better results, in the hypothesis of an improved charge separation efficiency. The exact sub-cellular unit involved in the ROS/Ca2+ interplay, driven by the NPs, should be also precisely identified. Finally, the effective modulation of intracellular Ca^{2+} second messenger in a non – apoptotic manner may affect important properties of excitable cells, such as differentiation and proliferation. Therefore, a similar study should be carried out with different cellular models, such as stem or neuronal ones.

APPENDIX A: THE VISION CASCADE *Principles of neuroscience, Kandell*

Human eye can be modelled as two interplaying parts: one, constituted by cornea and crystalline and the other constituted by the retina, shown in detail in figure A1. The former acts like a lens system, being responsible for focusing light rays in the point of higher acuity of the retina, that is the fovea. Here, photoreceptors are

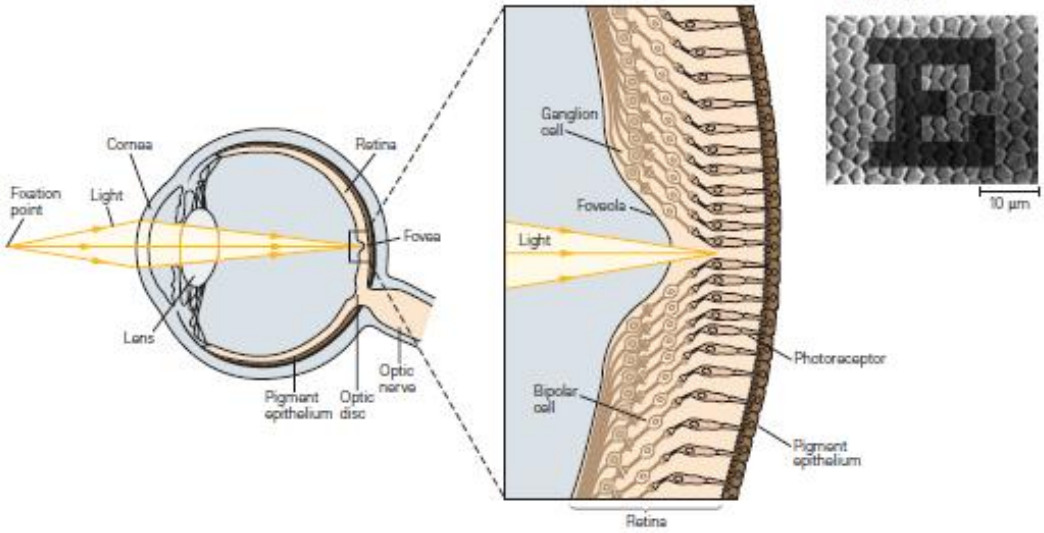

Figure A1: Scheme of the optical path in human eye, focus on the retina.

accommodated: they are neuronal like cells, which can be modelled as photodetectors, since they respond with a voltage stimulus after being hit by photons. The voltage drop is then read by bipolar cells, which generate another potential drop, that will be read by ganglion cells, the outing neurons of the retina. This system acts like a centre of analysis for the electrical stimuli generated ahead. Thus, the whole system can be modelled as shown in figure. Focusing on the fovea structure, is worth noting the reciprocal position of ganglion cells and photoreceptors: even if the latter are those which have to receive more light, they are located beside the neuronal system. The vision cascade can be schematized in three steps: first, photoreceptors are activated by incoming photons, then they activate a nucleotide, cyclic guanosine 3'-5' monophosphate (cGMP) that finally changes the ionic concentrations inside the photoreceptor, stimulating the generation of an action potential. The latter is peculiar of excitable cells, identified as a short event in which the membrane potential of the cell (in this case, of the photoreceptor) rises and falls. It is associated to the closure of ionic channels of the membrane, resulting in a different ionic concentration in the cell.

- Phase 1: activation of photoreceptors.

Photoreceptors contain visual pigments, composed of two molecules (proteins), retinal and opsin, only the former being light sensitive. It is a photochromic compound, since light absorption changes its conformation from cis to trans. This provokes the opening of the opsin site, that now is dispersed in the photoreceptor medium.

- Phase 2: closing of ionic channels.

The increase in concentration of opsin activates another protein, the trasducin, that is able to bind the cGMP. Since ionic channels such as Na+, K+ and Ca2+ are cGMP gated, the decrease in concentration of that protein provokes the closing of these ionic channels. The result is a higher concentration of cations inside the photoreceptor, whose membrane potential experiences the hyperpolarization (figure A2). When the light stops, the cGMP concentration goes back to its initial value, opening the ionic channels and restoring the initial value of the membrane potential.

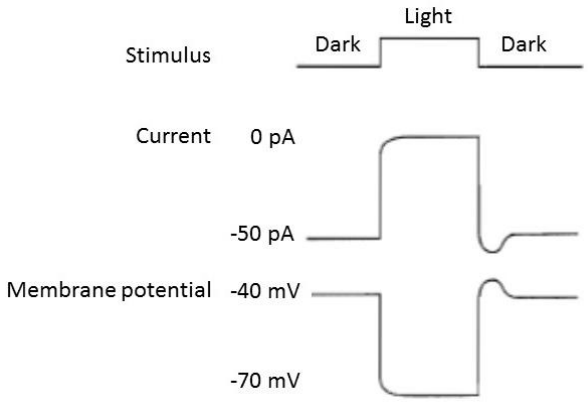

Figure A2: Response of membrane potential and current to light stimulus.

- Phase 3: bipolar and ganglion cells.

Photoreceptors are in contact with bipolar cells, whose role is to communicate with ganglion cells via synapsis. Ganglion cells are connected to optical nerve, that communicate with the brain for the analysis of the image.

Diseases like maculopathies affect the first phases of the vision cascade, disactivating the photoreceptors. For this reason, the role of the implant should mimic the one of the photoreceptors: absorption of light and generation of action potential to bipolar cells. Moreover, being the implant in the eye, no external voltage can be applied to the prosthesis; for these reasons, a photovoltaic panel offers an interesting solution. The prosthesis is made of an active material, being organic semiconductor, in

contact with bipolar cells, an acceptor and a conductive layer. Even if this device restored the vision acuity on blind rats, the mechanisms behind its action on phototransduction is still unclear. One of the hypothesis is the activation of chemical reactions able to interfere with the ionic channels of the bipolar cells, thus generating its action potential. The interaction between oxygen and polymer has been exploited in this view.

APPENDIX B: ELECTROCHEMICAL MEASUREMENTS *Electrochemical measurements, Bard – Faulkner*

An electrochemical measurement consists in determining the amount of charges generated by chemical species. The transport of charges happens through an interface between an ionic conductor, the electrolyte, and an electronic conductor, the electrode. Usually, the former is a liquid solution consisting of water and ionic species as H^+ or Cl^-, while the latter is a solid metal or semiconductor, like Pt or ITO. The electrode is put in the solution and connected to an external voltage generator, closing the circuit. The measure is performed by applying an external voltage and recording the amount of charges that passes through the circuit. Being the potential defined between two points, is necessary to use at least another electrode: usually, the one at which reactions are occurring is called working electrode, while the other is the reference electrode. Since the latter is taken as reference, there are three available choices which are at constant composition, their potentials being reported in table B1. Therefore, being the potential of those electrodes constant, it is changed at the working electrode with respect to the reference one. Now, let us consider the chemical species being in the solution: they can experience oxidation or reduction, or both,

Table B1.

Name	Potential
Normal Hydrogen Electrode (NHE)	0.00 V
Saturated Calomel Electrode (SCE)	0.242 V *vs* NHE
Silver – Silver chloride (Ag/AgCl)	0.197 V *vs* NHE

depending on the *standard potential* E^0 related to the pair. Let us consider an example: the reaction $Na^+ + e^- \rightarrow Na$ has a standard potential of E^0 = -2.71 V *vs* NHE, that

means that the electron must have an energy of 2.71 eV for promoting it. The sign is related to the flow of the charges (figure B1): when their movement is from the electrode to the electrolyte, the solution is reduced and the electrode is oxidized, therefore is called reduction current. Conversely, for electron flowing from the solution to the electrolyte, we have an oxidation current. The reduction current is obtained when a negative potential is applied between the working and the reference

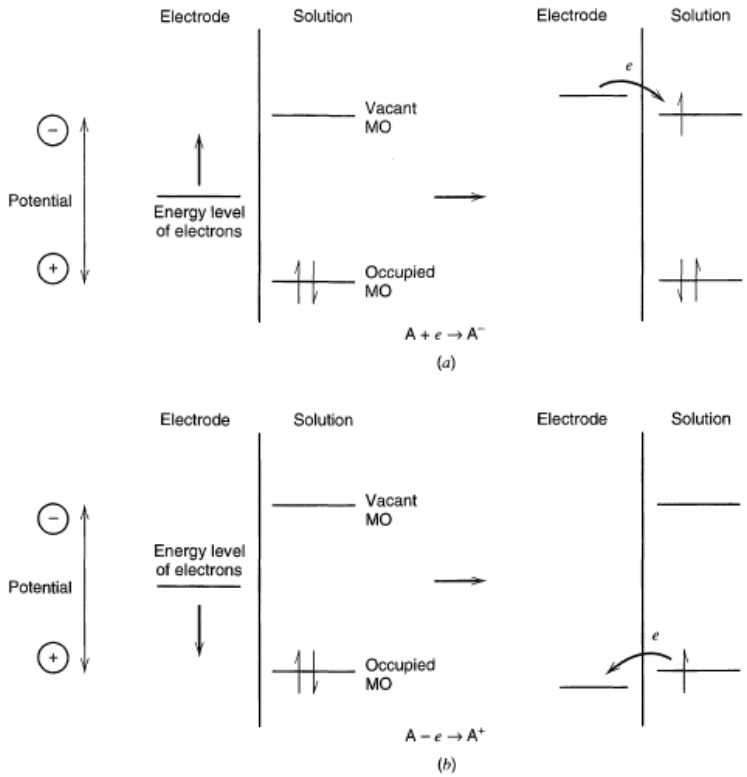

Figure B1: Reduction (a) and oxidation (b) currents in electrochemical measurements.

electrode: at a certain point, the potential will be associated to a high enough energy for electron's escape, that will find a lower energy state in the solution. Conversely, when a positive potential is applied between the working and the reference electrode, the electrons in the solution find a lower energy state in the electrode, thus solution oxidized. Reduction current experiences a flow of electrons from the working electrode to the solution, also called cathodic current; conversely, oxidation current experiences the movement of charges from solution to electrodes, also called anodic current. For historic reasons, the cathodic current is taken as positive, while the anodic one is negative. The current is measured between the two electrodes: a very simple electronic model provides a battery and a resistance, the latter being strongly dependent on the solution. Thus, the relation between current and voltage (I-V characteristic) is expected to be linear. The resistance of the solution can be very high; for dealing with this point, we have two solutions: one provides the help of a

supporting electrolyte, the other provides the introduction of a third electrode. Of course, both can be used contemporarily. The supporting electrolyte is an ionic solution, in general made of NaCl, that increases the conductivity of the solution itself, thus decreasing the R_s resistance. Usually, the standard potentials of the supporting electrolyte are known and far from the working potential range. When another electrode is used, we deal with a three elements cell, where the supporting electrode is called counter electrode. In this case, the current is measured between the counter and the working electrodes, while the potential is still applied between working and reference electrodes. In this way, the current and the potential are decoupled from R_s, even though a small uncompensated contribution still remains. The current associated to a redox couple is called faradaic process: in this case, the amount of products formed by charges is given by Faraday's law,

$$96485.4\ C\ generate\ 1\ mole\ of\ product \qquad (B1)$$

There are potential ranges in which electron transfer reactions are thermodynamically or kinetically unfavourable, so there is no current flow. Even though, processes like adsorption or desorption can occur, changing the structure of the electrode/solution interface, provoking a recorded current or voltage that is not related to charge flow: they are called non – faradaic processes. Is worth noting that those reactions are happening in the solution, for example being associated to ionic motion towards the electrodes, but they are not directly involving electron transfer with them: thus, they are recorded as transient currents. They must be considered when performing the experiment.

There are two kind of measurements that have been performed in this work: chronoamperometry and cyclic voltammetry, both with a three elements cell, with Pt as reference electrode and Ag/AgCl as counter electrode.

- Chronoamperometry: the cell is kept at an external voltage, then the current flow is measured while changing some conditions, for example illuminating the working electrode.
- Cyclic voltammetry: the cell's potential is linearly changed within a range of positive and negative values. In this way, both anodic and cathodic currents are recorded: peaks in the positive range of potential are related to reductions of the electrode, while peaks in the negative range of potential are due to oxidations.

References

[1] L. Spinelli, A. Torricelli, A. Pifferi, P. Taroni, G. M. Danesini, and R. Cubeddu, “Characterization of female breast lesions from multi-wavelength time-resolved optical mammography.,” *Phys. Med. Biol.*, vol. 50, no. 11, pp. 2489–502, 2005.

[2] L. F. De Freitas and M. R. Hamblin, “Proposed Mechanisms of Photobiomodulation or Low-Level Light Therapy,” *IEEE J. Sel. Top. Quantum Electron.*, vol. 22, no. 3, 2016.

[3] C. A. Robertson, D. H. Evans, and H. Abrahamse, “Photodynamic therapy (PDT): A short review on cellular mechanisms and cancer research applications for PDT,” *J. Photochem. Photobiol. B Biol.*, vol. 96, no. 1, pp. 1–8, 2009.

[4] I. V Fedotov *et al.*, “Fiber-optic control and thermometry of single-cell thermosensation logic.,” *Sci. Rep.*, vol. 5, p. 15737, 2015.

[5] K. Deisseroth, “Optogenetics,” *Nat. Methods*, vol. 8, no. 1, pp. 26–29, 2011.

[6] M. Irie, T. Fukaminato, K. Matsuda, and S. Kobatake, “Photochromism of diarylethene molecules and crystals: Memories, switches, and actuators,” *Chem. Rev.*, vol. 114, no. 24, pp. 12174–12277, 2014.

[7] “Kandel. Principi di Neuroscienze. 3_underlined.pdf.” .

[8] D. Ghezzi *et al.*, “A polymer optoelectronic interface restores light sensitivity in blind rat retinas,” *Nat. Photonics*, vol. 7, no. 5, pp. 400–406, 2013.

[9] E. Zucchetti *et al.*, “Poly(3-hexylthiophene) nanoparticles for biophotonics: study of the mutual interaction with living cells,” *J. Mater. Chem. B*, 2016.

[10] W. H. De Jong and P. J. a Borm, “Drug delivery and nanoparticles:applications and hazards.,” *Int. J. Nanomedicine*, vol. 3, no. 2, pp. 133–149, 2008.

[11] E. Mosconi *et al.*, “Surface Polarization Drives Photoinduced Charge Separation at the P3HT/Water Interface,” *ACS Energy Lett.*, vol. 1, no. 2, pp. 454–463, 2016.

[12] E. Lanzarini *et al.*, “Polymer-Based Photocatalytic Hydrogen Generation,” *J. Phys. Chem. C*, vol. 116, no. 20, pp. 10944–10949, 2012.

[13] N. Martino *et al.*, “Photothermal cellular stimulation in functional bio-polymer interfaces.,” *Sci. Rep.*, vol. 5, p. 8911, 2015.

[14] S. Bellani *et al.*, “Reversible P3HT/Oxygen Charge Transfer Complex Identi fi cation in Thin Films Exposed to Direct Contact with Water,” *J. Phys. Chem. C*, vol. 118, pp. 6291–6299, 2014.

[15] C. Tortiglione *et al.*, “Semiconducting polymers are light nanotransducers in eyeless animals,” *Sci. Adv.*, vol. 3, no. 1, 2017.

[16] K. Krumova and G. Cosa, “Chapter I: Overview of reactive oxygen species,” *Singlet Oxyg. Appl. Biosci. Nanosci. Vol. 1*, p. 21, 2016.

[17] D. V. Sakharov, E. D. R. Elstak, B. Chernyak, and K. W. A. Wirtz, “Prolonged lipid oxidation after photodynamic treatment. Study with oxidation-sensitive probe C11-BODIPY581/591,” *FEBS Lett.*, vol. 579, no. 5, pp. 1255–1260, 2005.

[18] A. Görlach, K. Bertram, S. Hudecova, and O. Krizanova, “Calcium and ROS: A mutual interplay,” *Redox Biol.*, vol. 6, pp. 260–271, 2015.

[19] J. Boyle, “Lehninger principles of biochemistry (4th ed.): Nelson, D., and Cox, M.,” *Biochem. Mol. Biol. Educ.*, vol. 33, no. 1, pp. 74–75, 2005.

[20] P. S. Brookes, Y. Yoon, J. L. Robotham, M. W. Anders, and S.-S. Sheu, “Calcium, ATP, and ROS: a mitochondrial love-hate triangle,” *AJP Cell Physiol.*, vol. 287, no. 4, pp. C817–C833, 2004.

[21] A. Gomes, E. Fernandes, and J. L. F. C. Lima, “Fluorescence probes used for detection of reactive oxygen species,” *J. Biochem. Biophys. Methods*, vol. 65, no. 2–3, pp. 45–80, 2005.

[22] K. ichi Setsukinai, Y. Urano, K. Kakinuma, H. J. Majima, and T. Nagano, “Development of novel fluorescence probes that can reliably detect reactive oxygen species and distinguish specific species,” *J. Biol. Chem.*, vol. 278, no. 5, pp. 3170–3175, 2003.

[23] N. Pirotte *et al.*, “Reactive oxygen species in planarian regeneration: An upstream necessity for correct patterning and brain formation,” *Oxid. Med. Cell. Longev.*, vol. 2015, 2015.

[24] J. M. Cooper, K. R. Greenough, and C. J. McNeil, “Direct electron transfer reactions between immobilized cytochrome c and modified gold electrodes,” *J. Electroanal. Chem.*, vol. 347, no. 1–2, pp. 267–275, 1993.

[25] C. Hidalgo and P. Donoso, “Crosstalk between calcium and redox signaling: from molecular mechanisms to health implications,” *Antioxid Redox Signal*, vol. 10, no. 7, pp. 1275–1312, 2008.

[26] Y. Yan, C. L. Wei, W. R. Zhang, H. P. Cheng, and J. Liu, “Cross-talk between calcium and reactive oxygen species signaling,” *Acta Pharmacol. Sin.*, vol. 27, no. 7, pp. 821–826, 2006.

[27] S. Bánsághi *et al.*, “Isoform- and species-specific control of inositol 1,4,5-trisphosphate (IP3) receptors by

reactive oxygen species," *J. Biol. Chem.*, vol. 289, no. 12, pp. 8170–8181, 2014.
[28] C. J. Mcneil, K. R. Greenough, P. A. Weeks, and C. H. Self, "ELECTROCHEMICAL SENSORS FOR DIRECT," vol. 17, no. 6, pp. 399–406, 1992.
[29] S. Nam, H. Kim, P. Degenaar, C. S. Ha, and Y. Kim, "Extremely slow photocurrent response from hemoprotein films in planar diode geometry," *Appl. Phys. Lett.*, vol. 101, no. 22, 2012.
[30] S. Nam, H. Kim, and Y. Kim, "Bias-dependent photocurrent response in protein nanolayer-embedded solid state planar diode devices.," *Nanoscale*, vol. 2, no. 5, pp. 694–6, 2010.
[31] Y. Wenger, W. Buzgariu, S. Reiter, and B. Galliot, "Injury-induced immune responses in Hydra," *Semin. Immunol.*, vol. 26, no. 4, pp. 277–294, 2014.

Acknowledgments

I have to thank Dr. Maria Rosa Antognazza and prof. Guglielmo Lanzani, for supporting and trusting me during this period. Your support has been fundamental for my personal and academic growth.

I want to thank my colleagues. Thank you Catia, for not killing me and my forgetfulness and for all the biology I learnt with you. Thank you Tullii, for being next to me with the *obscura* chemistry and diabolic electrochemistry. Thank you Desii, for your help with the images. Thank you, Francesco, Isabella and Elena.

I have to thank my old friends, who have been close to me during all these years. Thank you, Elisa, for your ability of making me smile. Special thanks to Giorgia and Elena. Thank you Stefanosem, for all your cries and our time, always spent in understanding physics. Thank you Giamp, for all the mathematics we learnt together.

A sincere thanks to Lidia, always with the right bottle at the right moment and for always having time to spend with me.

A special thanks to my family: mother, father and Zena, you made this dream come true. Thank you for supporting me in all my “I want to die”, for always being there for me.

In the end, thanks go to my beloved Giovanni, example of knowledge and hard work.